Supplementary Material

Glacial–interglacial cycles in the south–central and south-eastern Pyrenees since ~180 ka (NE Spain-Andorra-SE France)

Valenti Turu[1,2,3,4*], Jose Luís Peña-Monné [5], Pedro P. Cunha [6], Guy Jalut[1], Jan-Pieter Buylaert [7], Andrew S. Murray [8], David Bridgland [9], Mads Faurschou-Knudsen[10], Marc Oliva[4], Rosa M. Carrasco[2], Xavier Ros[1], Laia Turu-Font [11], Josep Ventura [1,3,4]

[1] Marcel Chevalier Earth Science Foundation, Andorra la Vella, Principat d'Andorra

[2] Departament of Geological and Mining Engineering, Castilla-La Mancha University, Spain

[3] Departamento de Dinámica de la Tierra y el Océano, Facultad de Ciencias de la Tierra, Universidad de Barcelona, Spain

[4] ANTALP (Antarctic, Arctic and Alpine Environments), Department of Geography, Barcelona University, Spain

[5] Departamento de Geografía y Ordenacion del Territorio and IUCA, Universidad de Zaragoza, Zaragoza, Spain

[6] University of Coimbra, MARE - Marine and Environmental Sciences Centre, Department of Earth Sciences, Coimbra, Portugal

[7] Department of Physics, Technical University of Denmark, Risø Campus, Denmark

[8] Nordic Laboratory for Luminescence Dating, Aarhus University, Risø DTU, Denmark

[9] Department of Geography, Durham University, Stackton Road, DH1 3LE England, UK

[10] Department of Geoscience, Aarhus University, Denmark

[11] Departament de Ciències de l'Antiguitat i l'Edat Mitjana, Universitat Autònoma de Barcelona, Spain

INDEX

1 GRAIN SIZE CHARACTERIZATION

The grain size characteristics (**Fig. SM1** and **SM2**) were obtained by using GRADISTAT software (Blott and Pye, 2001). The sediment samples correspond from very coarse sands to fine silts (**Table SM1**). They are dominated by the sand fraction (2 mm - 63 μm), ranging from 95-47 %, except for sample GINEBROSA which is dominated by the silt fraction (63 - 4 μm) – 75 %. Some samples have fractions of pebbles (>4 mmm) and granules (4-2 mm). The samples are unimodal (with the exception of samples VILALLER-1 and LMARG-1), with standard deviation indicating to be poorly sorted, with positive asymmetry and very leptokurtic to mesokurtic (**Table SM2**). The grain-size distribution and statistical parameters of the samples may be from tractive transport and deposition by water or wind and gravity; however, also within diluted turbidites or mud flows like for sample GINEBROSA. Despite the grain-size characteristics of all samples, the obtained estimated OSL ages should not be affected by residual doses at the moment of deposition; nevertheless, we look at this question after the following sample's description.

The fluvial deposits from Cerdagne (Sanavastre and Ur) are moderately well sorted (**Fig. SM3**, SANAV-1) or very well sorted (**Fig. SM4**, SANAV-2 and **Fig. SM5**, UR-1), also from Adrall at the Urgellet (**Fig. SM6**, ADRALL-4). However, the current river bed-load in Cerdagne (**Fig. SM7**, SANAV-0) is moderately sorted, and the kame deposits from Segudet (**Fig. SM8**, SEGUDET-1). Glacio-fluvial deposits related to till complexes are poorly sorted, like in Vilaller (**Fig. SM9**, VILALLER-1 and **Fig. SM10**, VILALLER-2); Sort (**Fig. SM11**, SORT-1); Santa Coloma (**Fig. SM12**, St.COLOMA-1); La Margineda (**Fig. SM13**, LMARG-1) and Sant Julià de Lòria (**Fig. SM14**, Stª JULIA-1). Mixed environments like colluvium and glacio-fluvial kame deposits produce poor sorted sands (**Fig. SM15**, GINEBROSA).

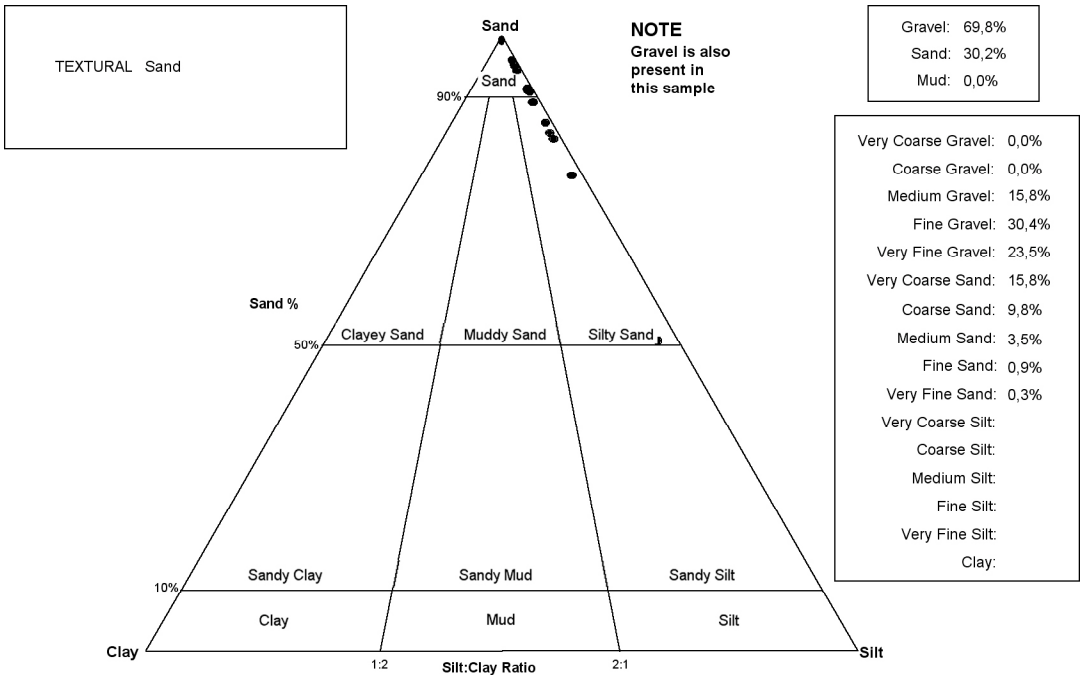

Fig. SM1 – Grain-size distribution in the Sand – Silt – Clay diagram. The majority of the samples are sands or silty-sands.

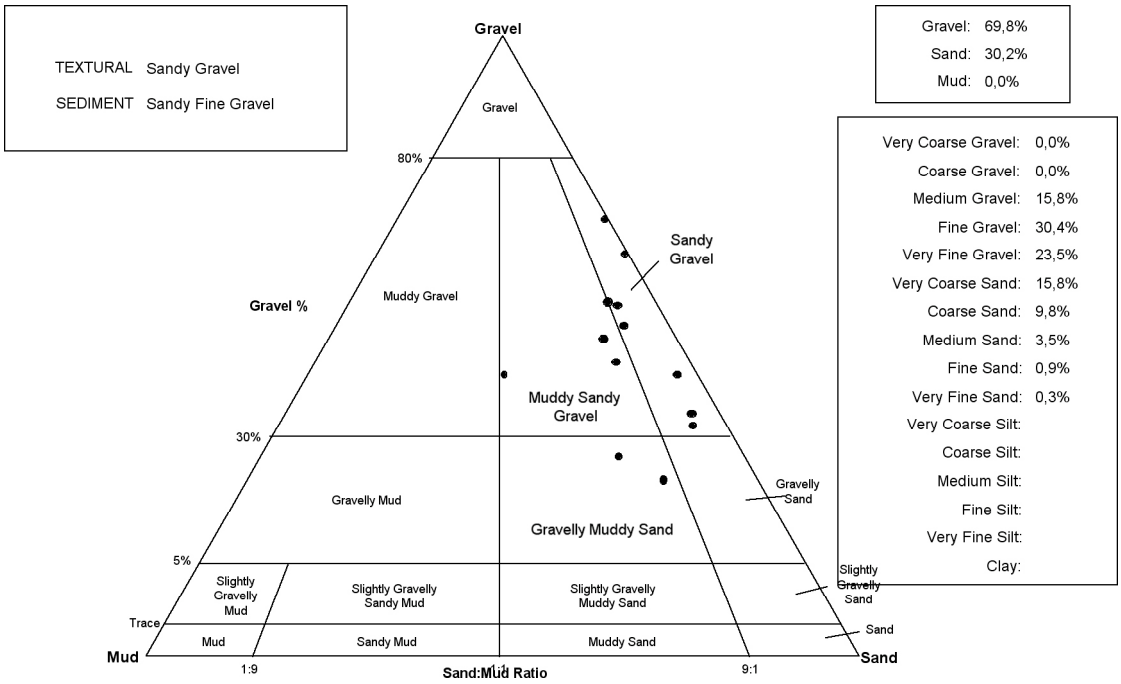

Fig. SM2 – Distribution in the Gravel – Sand – Mud diagram. The majority of the samples are sandy-gravels or muddy-sandy-gravels, but also a few are gravelly-muddy-sands.

		Pebbles	Granules	Sand	Silt	Clay	Fines	Mean	Median	Mode	S.Deviation	Assimetry	Kurtosis
NLL-Risø code	Sample	>4 mm (%)	4-2 mm (%)	200-63µm (%)	63-4µm (%)	<4µm (%)	<63µm (%)	mm	mm	mm			
122235	SANAV-0	14.30	21.72	63.21	–	–	0.77	1.25	0.95	1.40	1.53	0.09	2.27
122236	SANAV-1	0.75	0.32	93.34	4.09	0.96	5.05	0.27	0.22	0.25	1.47	2.17	12.31
122237	SANAV-2	0.26	1.13	95.06	2.75	0.45	3.20	0.35	0.25	0.25	1.22	2.40	15.96
122238	VILALLER-1	20.97	11.16	61.03	4.78	1.56	6.34	0.69	0.45	0.25	2.72	0.72	3.86
122239	VILALLER-2	0.58	1.84	45.28	42.04	5.89	47.93	0.05	0.05	0.06	2.40	0.25	3.58
122240	UR-1	1.47	10.25	87.30	–	–	0.99	0.93	0.64	0.71	0.98	0.37	4.20
122241	SORT-1	0.55	8.75	82.60	6.29	1.05	7.34	0.45	0.36	0.50	2.01	1.56	6.59
122242	StªCOLOMA-1	10.32	10.49	72.41	4.85	1.23	6.08	0.52	0.37	0.25	2.37	0.76	4.44
122243	LMARG-1	26.90	8.22	47.44	13.96	2.19	16.15	0.53	0.37	7.92	3.37	0.44	2.46
122244	Stª JULIA-1	3.88	1.92	76.10	13-13	3.94	17.07	0.18	0.17	0.25	2.59	0.79	3.96
122245	SEGUDET-1	–	–	81.36	13.58	2.08	15.66	0.12	0.11	0.13	1.77	1.62	6.12
122246	FAUCELLES	–	–	–	70.5	29.5	100,00	0.005	0.004	0.006	1.29	0.42	2.86
122247	ADRAL-4	–	0.11	95.17	3.68	0.59	4.27	0.33	0.27	0.36	1.30	2.84	14.71
122248	STPCodinet-1	31.49	12.72	55.13	0.57	0.09	0.66	0.18	0.36	5.61	3.9	0.15	1.62
122256	GINEBROSA	–	–	6.44	75.06	13.85	88.91	0.01	0.01	0.03	1.86	0.71	2.76

Table SM1 – Results of the grain-size analysis of the NLL or Risø studied sediment samples.

NLL – Risø code	Sample	Classification
122235	SANAV-0	Coarse to very coarse sand, moderately sorted, symmetrical and mesokurtic
122236	SANAV-1	Medium sand, moderately well sorted, very coarse skewed and very leptokurtic
122237	SANAV-2	Medium sand, very well sorted, very coarse skewed and very leptokurtic
122238	VILALLER-1	Medium to coarse sand poorly sorted, coarse skewed and mesokurtic
122239	VILALLER-2	Sand-silty poorly sorted, symmetrical and leptokurtic
122240	UR-1	Coarse sand very well sorted, symmetrical and leptokurtic
122241	SORT-1	Medium sand poorly sorted, very coarse skewed and leptokurtic
122242	StªCOLOMA-1	Medium to coarse sand poorly sorted, coarse skewed and leptokurtic
122243	LMARG-1	Medium to coarse pebbly sand poorly sorted, coarse skewed and platykurtic
122244	Stª JULIA-1	Fine to medium sand poorly sorted, coarse skewed and leptokurtic
122245	SEGUDET-1	Very fine to fine sand moderately sorted, very coarse skewed and leptokurtic
122246	FAUCELLES	Very fine silt, well sorted, symmetrical and mesokurtic
122247	ADRAL-4	Medium sand well sorted and very coarse skewed, leptokurtic
122248	STPCodinet-1	Fine-medium sand plus pebbles, poorly sorted, symmetrical & very platykurtic
122256	GINEBROSA	Fine to medium silt moderately sorted and coarse skewed, mesokurtic

Table SM2 – Classification of the statistical parameters obtained from the particle size distributions.

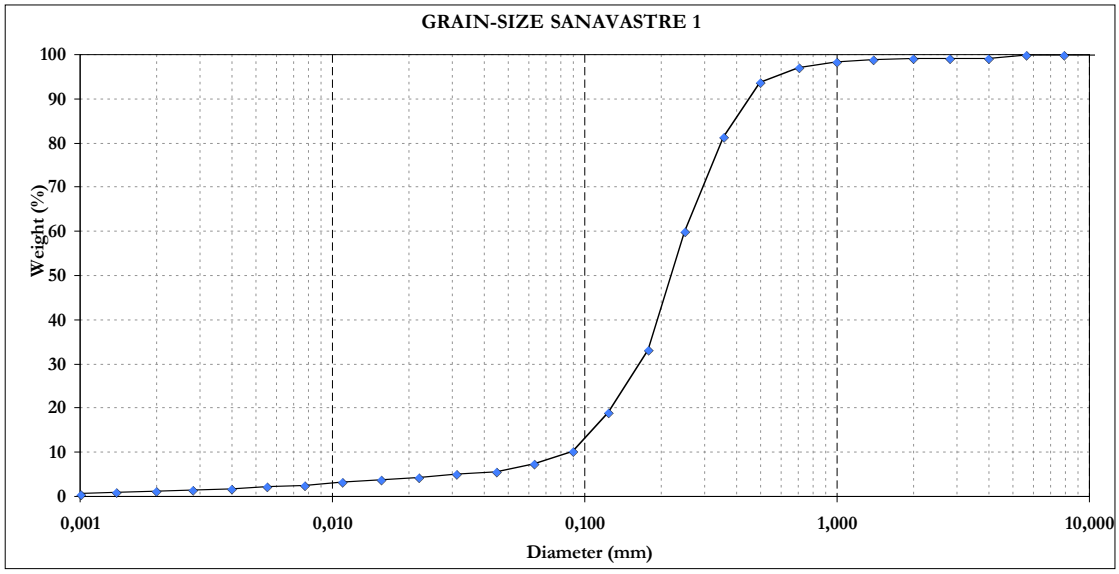

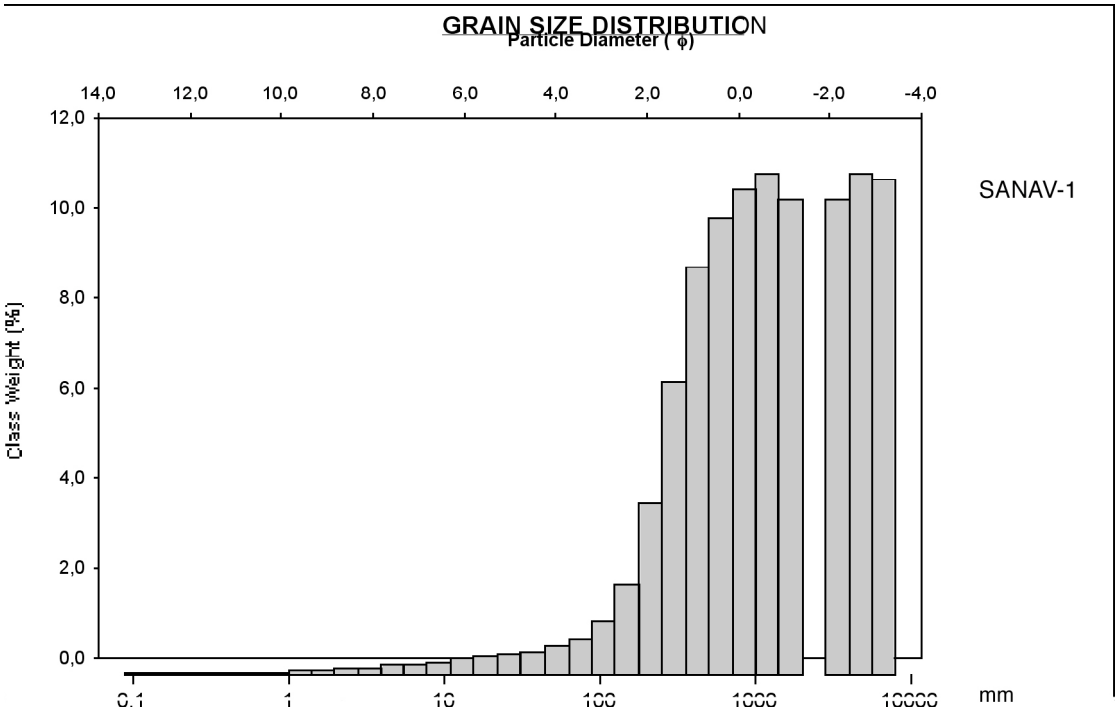

Fig. SM3 – On top cumulative frequency curve of sample SANAV-1. Sanavastre in the Cerdagne. Histogram: poorly sorted sandy fine gravel sample or very coarse sand, symmetrical and platykurtic bimodal distribution for SANAV-1. Only for unimodal samples the sorting, skewness and kurtosis are therefore reliable.

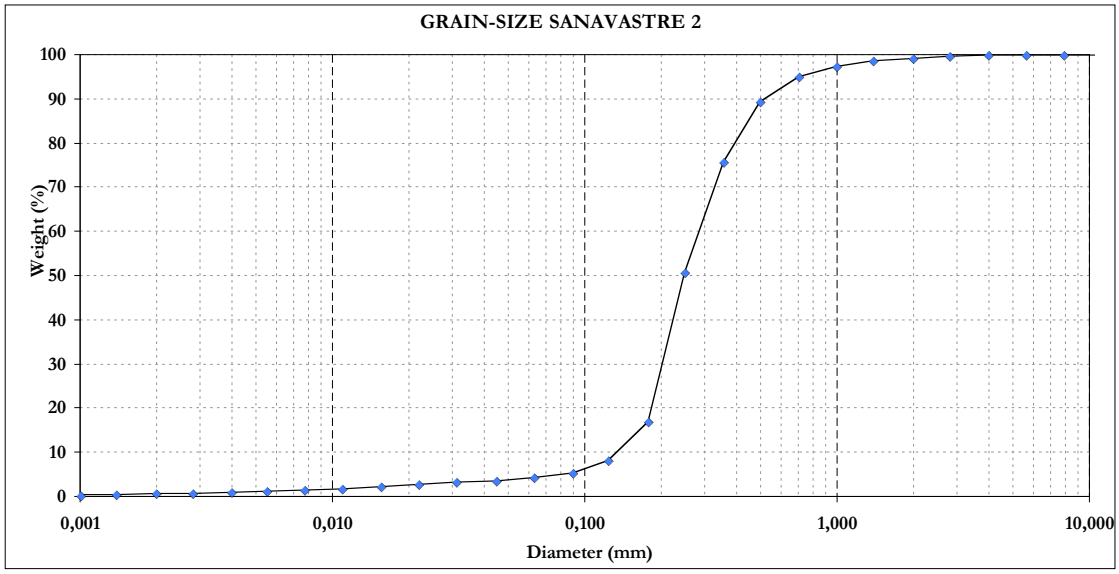

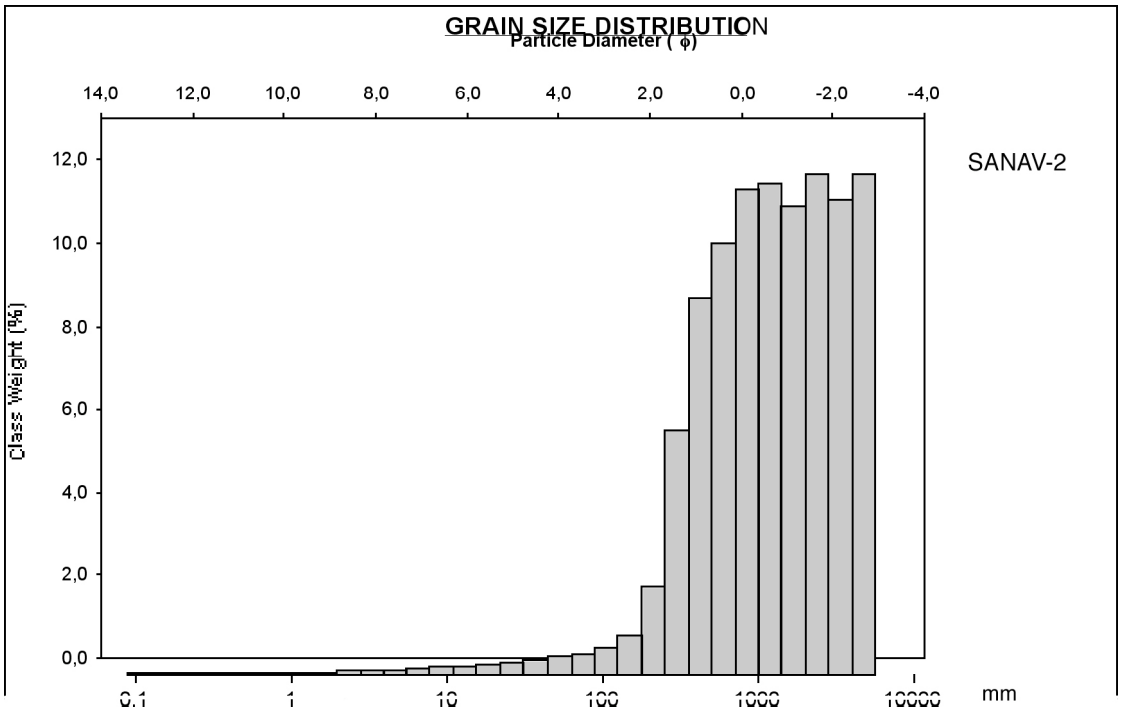

Fig. SM4 – On top, cumulative frequency curve of sample SANAV-2. Sanavastre in the Cerdagne. Histogram: poorly sorted very coarse sand or sandy very fine gravel, fine skewed and platykurtic. Trimodal distribution for SANAV-2 sample. Only for unimodal samples the sorting, skewness and kurtosis are therefore reliable.

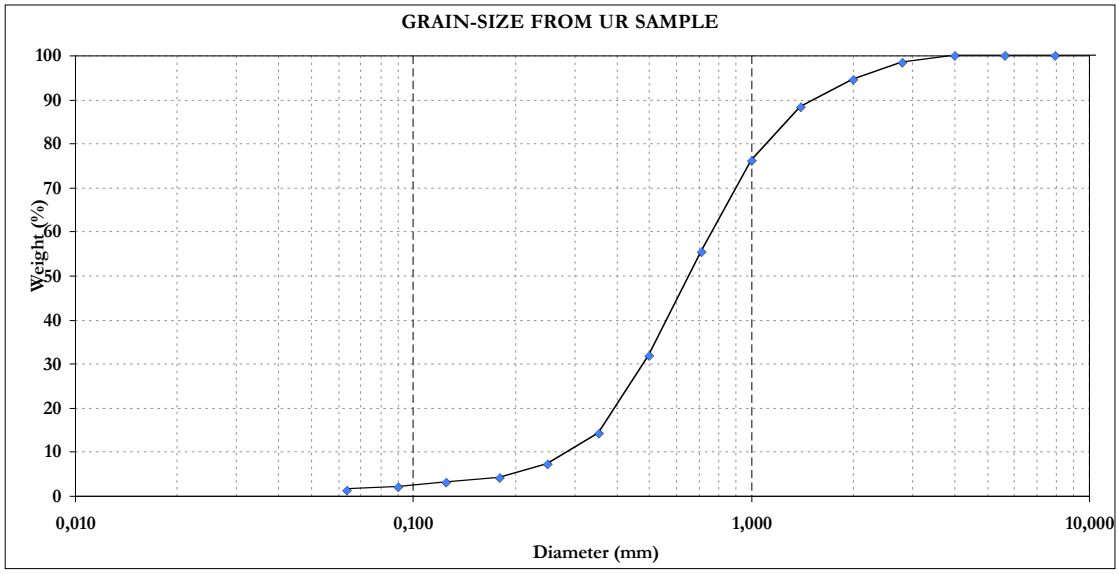

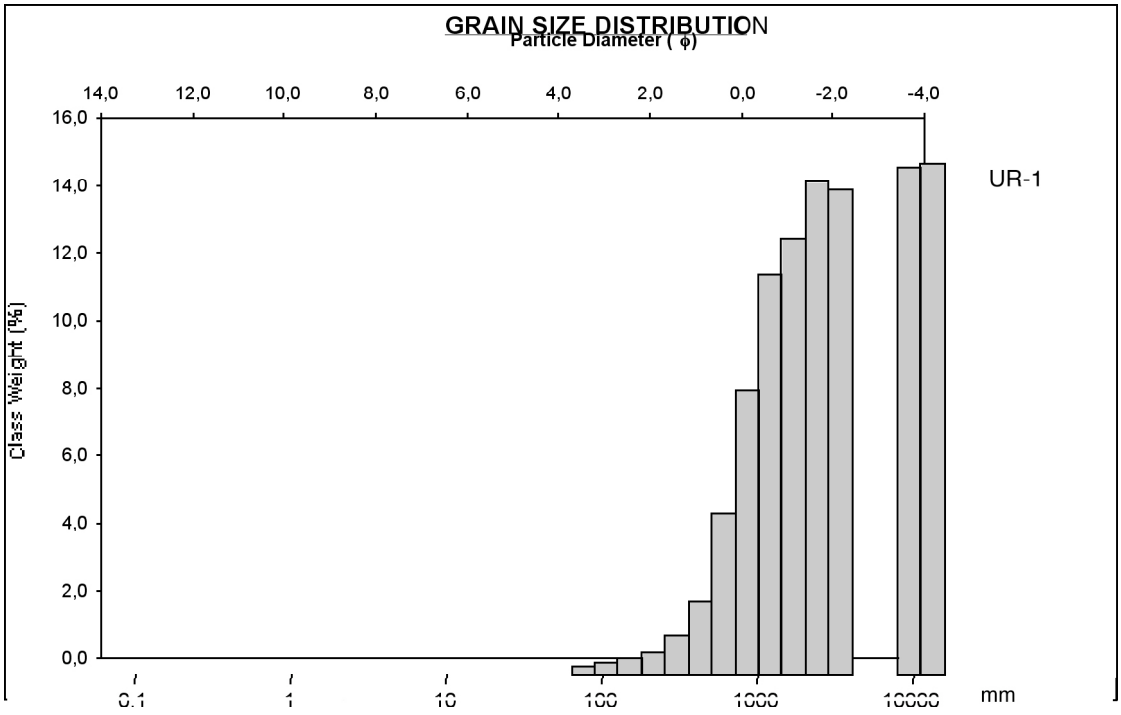

Fig. SM5 – On top, cumulative frequency curve of sample UR-1. Ur terrace in the Cerdagne. Histogram: Poorly sorted sandy medium gravel or very fine gravel, very fine skewed, very platykurtic. Bimodal distribution for UR-1 sample. Only for unimodal samples the sorting, skewness and kurtosis are therefore reliable.

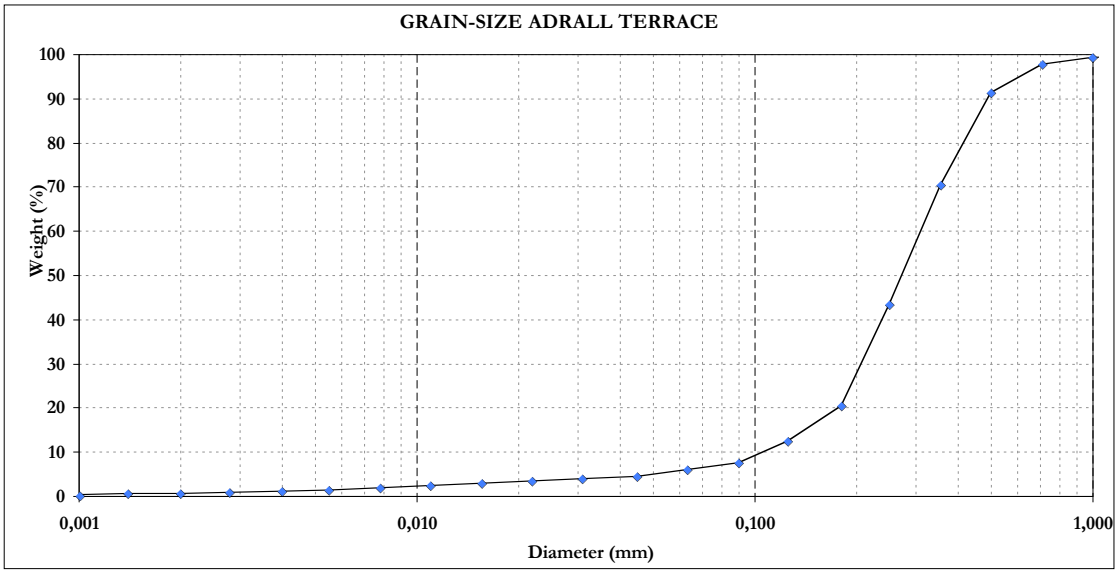

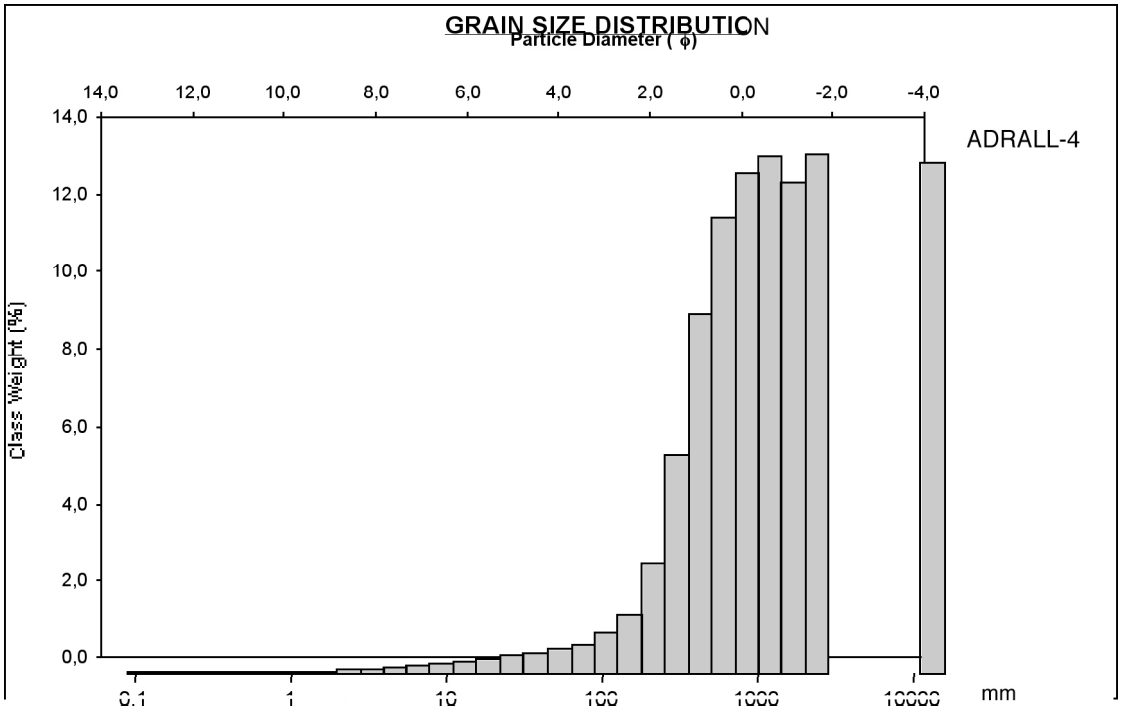

Fig. SM6 – On top, cumulative frequency curve of sample ADRALL-4. Segre fluvial terrace at Urgellet. Histogram: Sandy medium gravel or very coarse sand, poorly sorted, symmetrical and platykurtic. Trimodal distribution for UR-1 sample. Only for unimodal samples the sorting, skewness and kurtosis are therefore reliable.

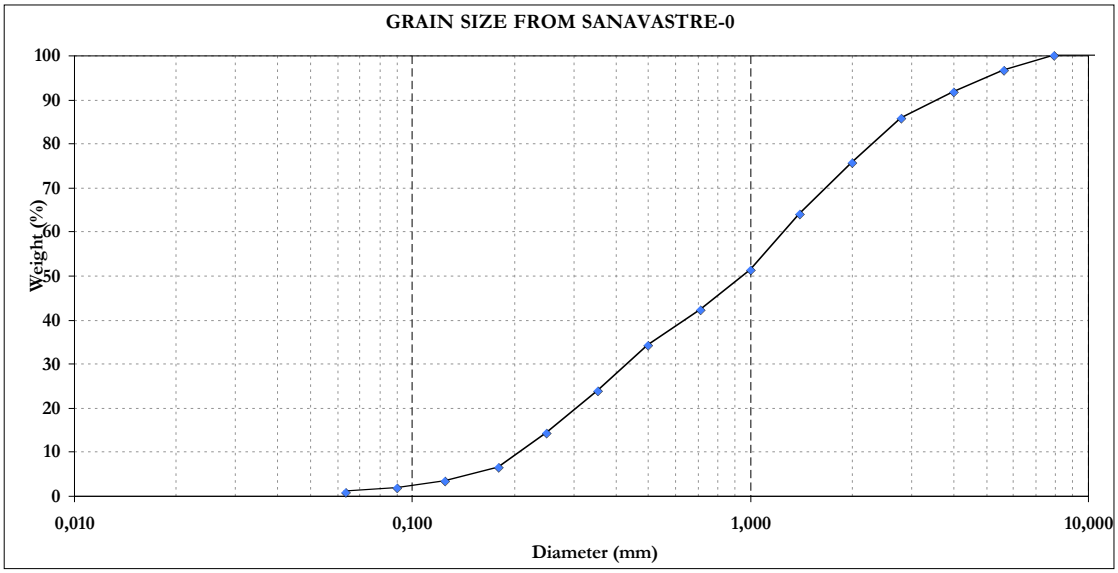

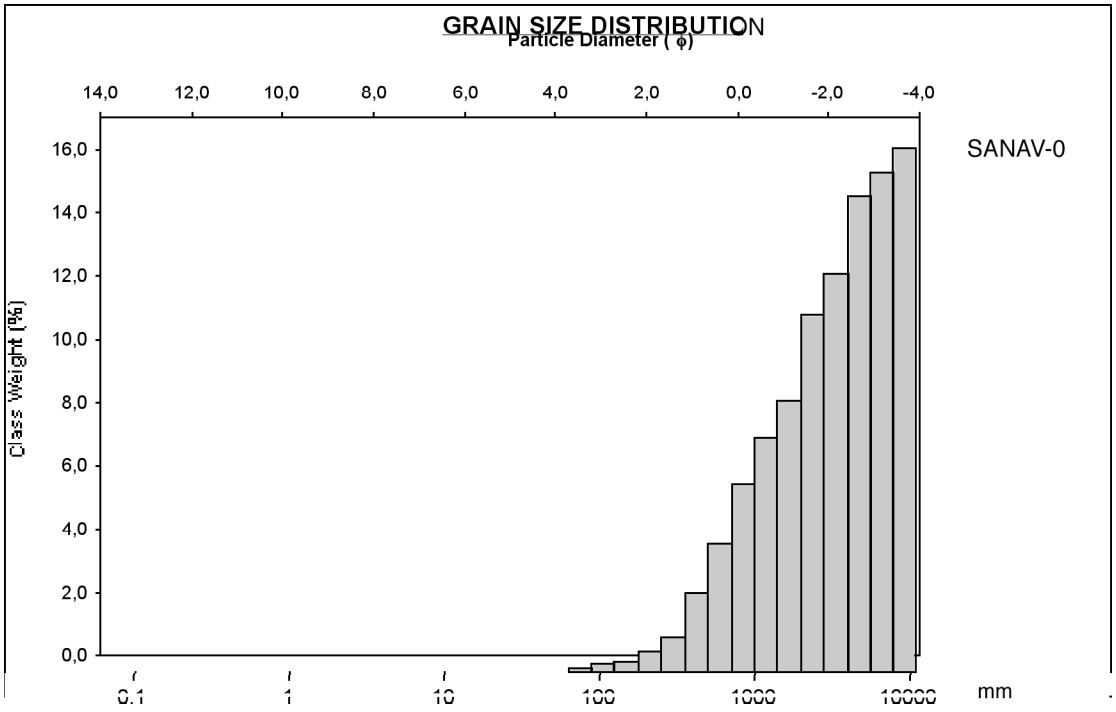

Fig. SM7 – On top, cumulative frequency curve of sample SANAV-0. Segre river bed in the Cerdagne. Grain-size histogram from SANAV-0, an unimodal distribution for the current Segre bed-load. Classification as sandy fine gravel to very fine gravel, poorly sorted, fine skewed and platykurtic.

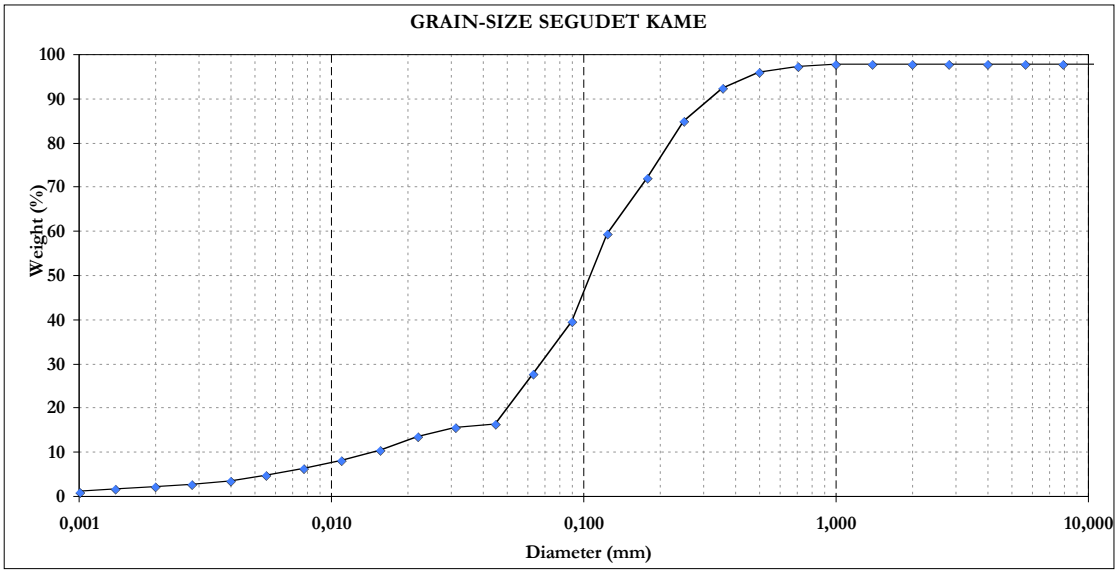

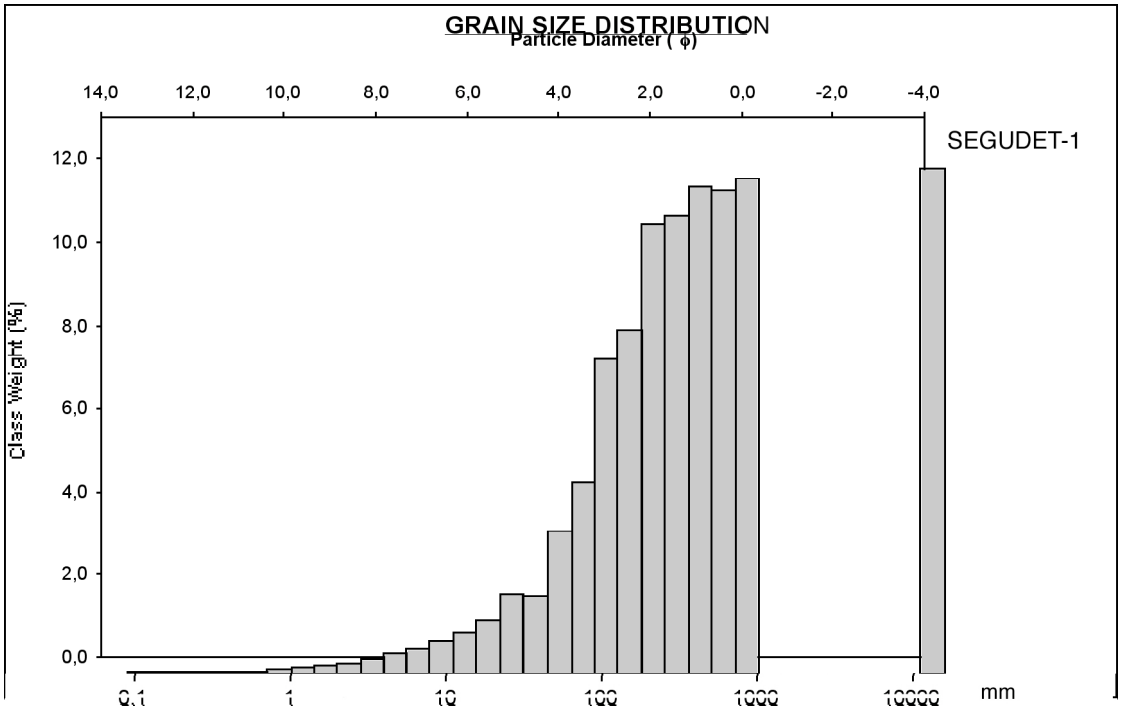

Fig. SM8 – On top, cumulative frequency curve of sample SEGUDET-1. Segudet kame complex in the Valira del Nord Valley. Histogram: Gravelly muddy sand or medium gravelly very coarse silty coarse sand, very poorly sorted, coarse skewed and leptokurtic. Polymodal distribution for SEGUDET-1 sample. Only for unimodal samples the sorting, skewness and kurtosis are therefore reliable.

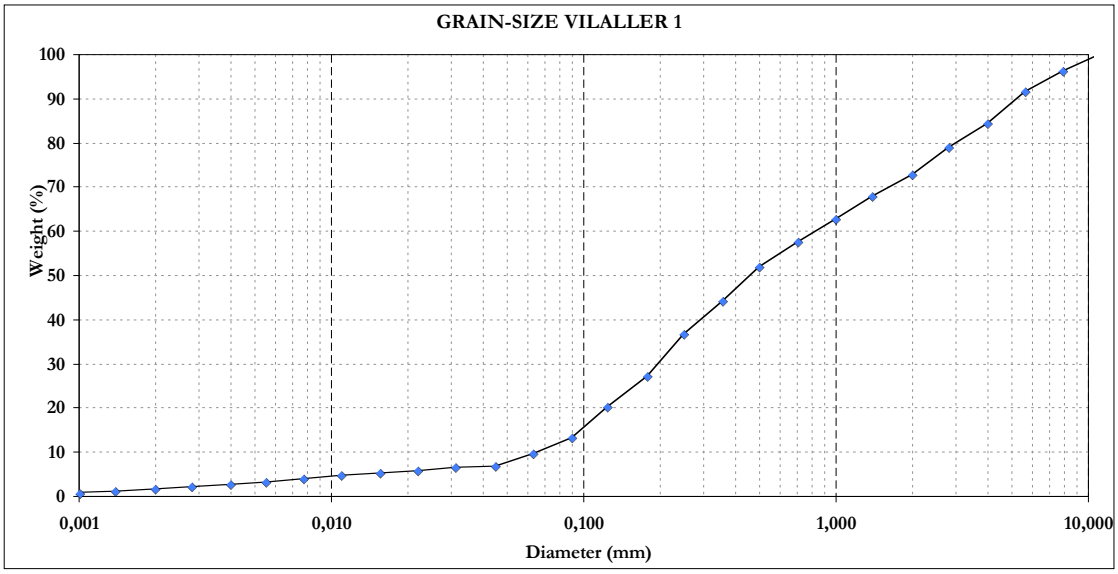

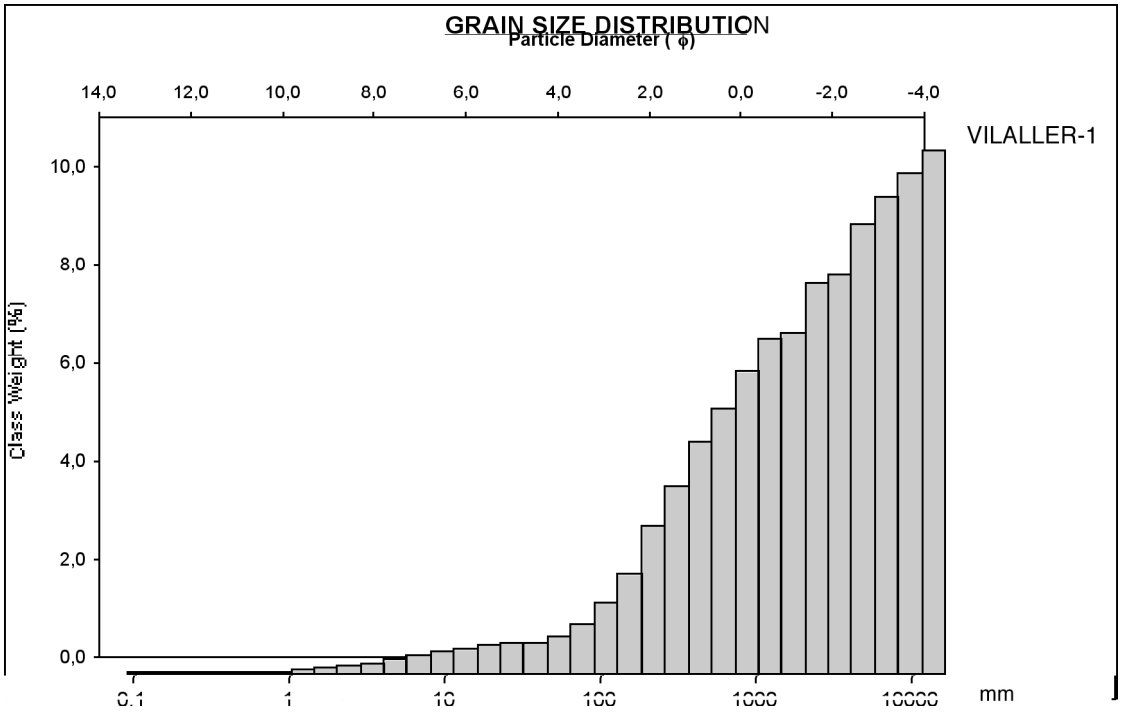

Fig. SM9 – On top, cumulative frequency curve of sample VILALLER-1. Sant Mames glacifluvial deposits, Vilaller in the Noguera Ribagorzana. Histogram: Muddy sandy gravel or very coarse silty sandy medium gravel, very poorly sorted, fine skewed, mesokurtic. Unimodal distribution for SEGUDET-1 sample.

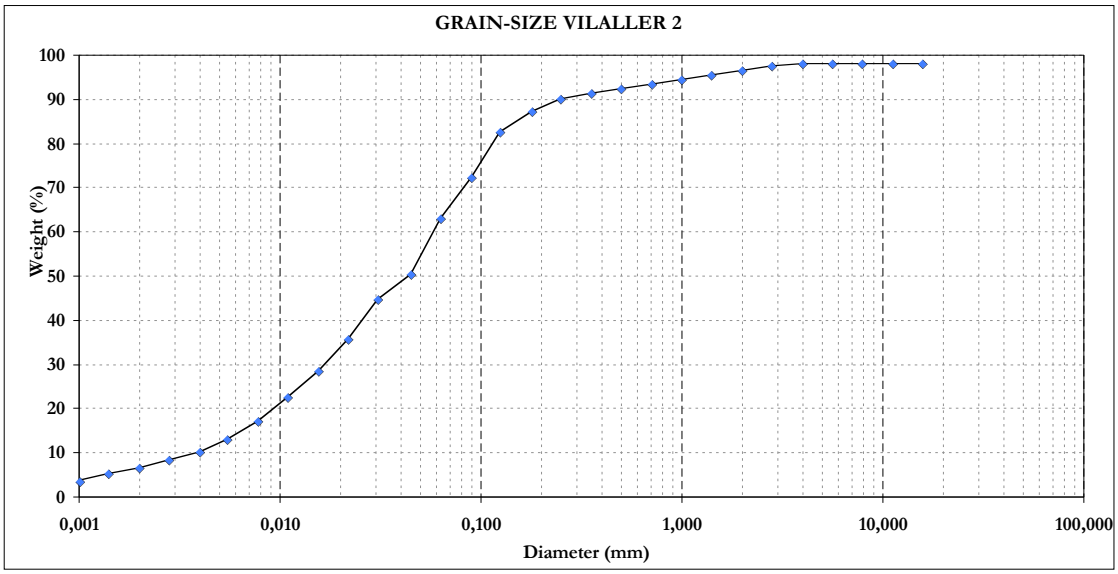

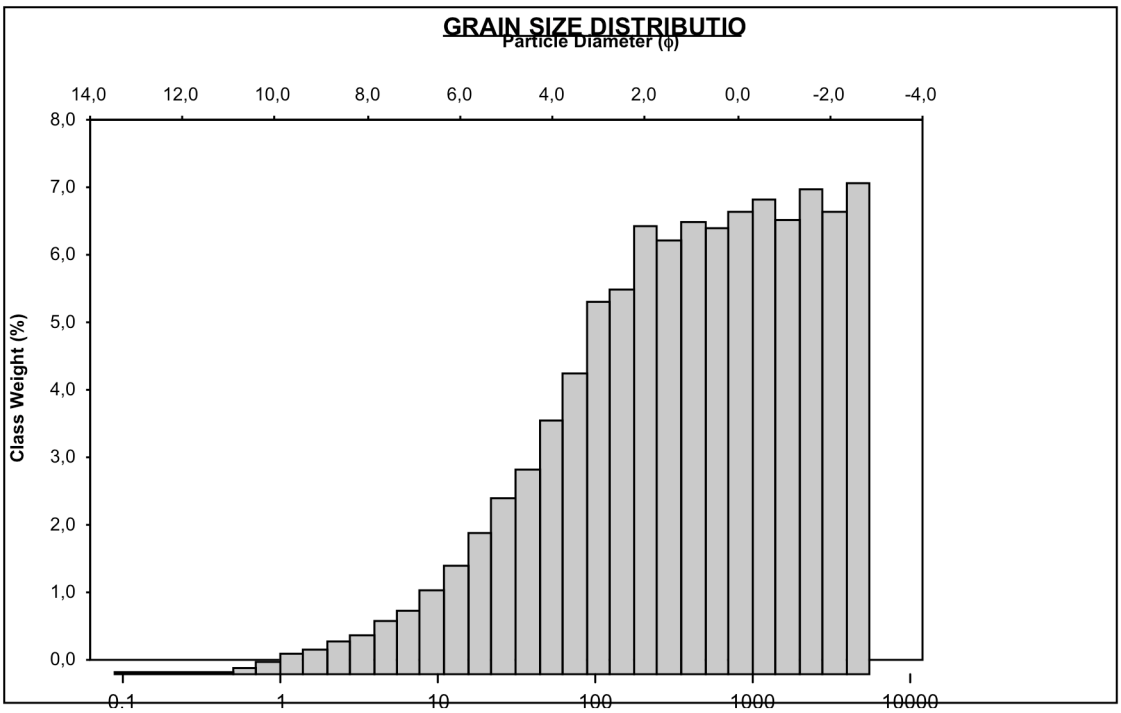

Fig. SM10 – On top, cumulative frequency curve of sample VILALLER-2. Sant Mames melt-out till deposits, Vilaller in the Noguera Ribagorzana. Histogram: Gravelly muddy sand or very fine gravelly very coarse silty very coarse sand, very poorly sorted, fine skewed, mesokurtic. Polymodal distribution for VILALLER-2 sample. Only for unimodal samples the sorting, skewness and kurtosis are therefore reliable.

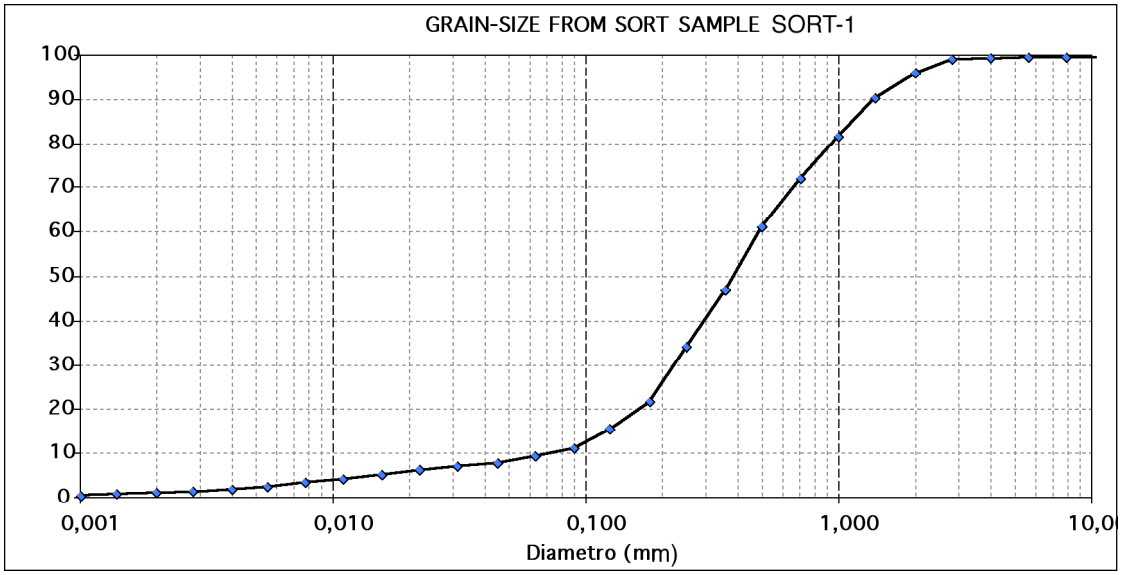

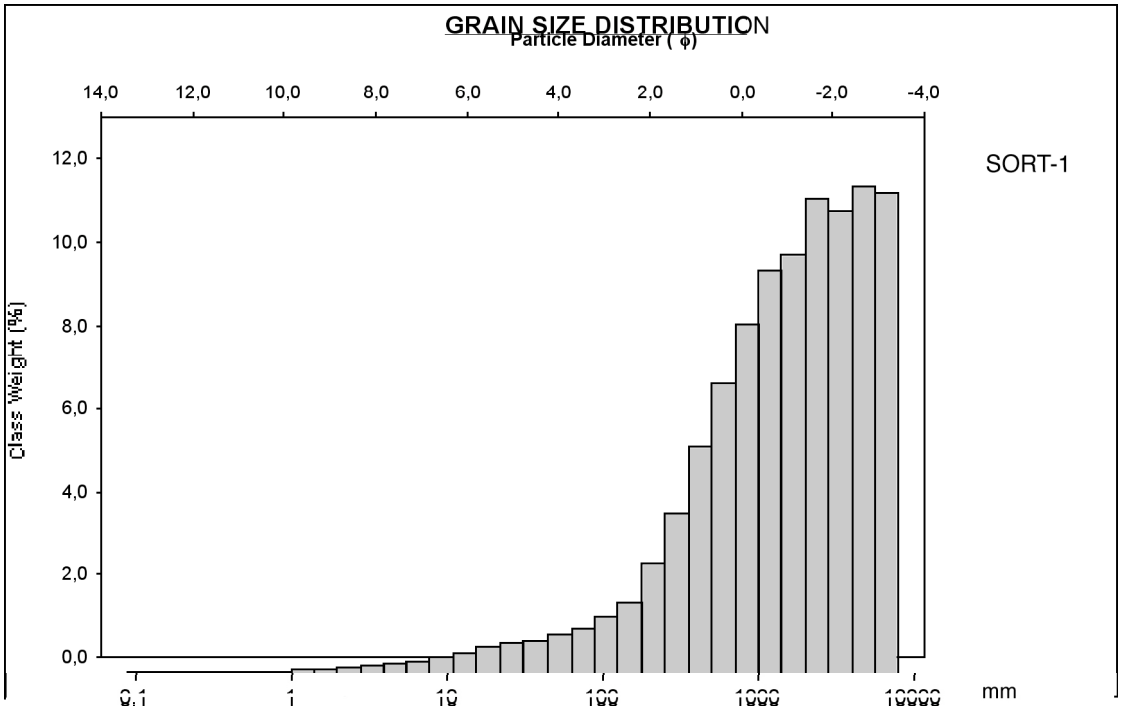

Fig. SM11 – On top, cumulative frequency curve of sample SORT-1. Sort terrace in the Noguera Pallaresa. Histogram: Sandy fine gravel or very coarse sand, poorly sorted, very fine skewed, platykurtic. Bimodal distribution for SORT-1 sample. Only for unimodal samples the sorting, skewness and kurtosis are therefore reliable.

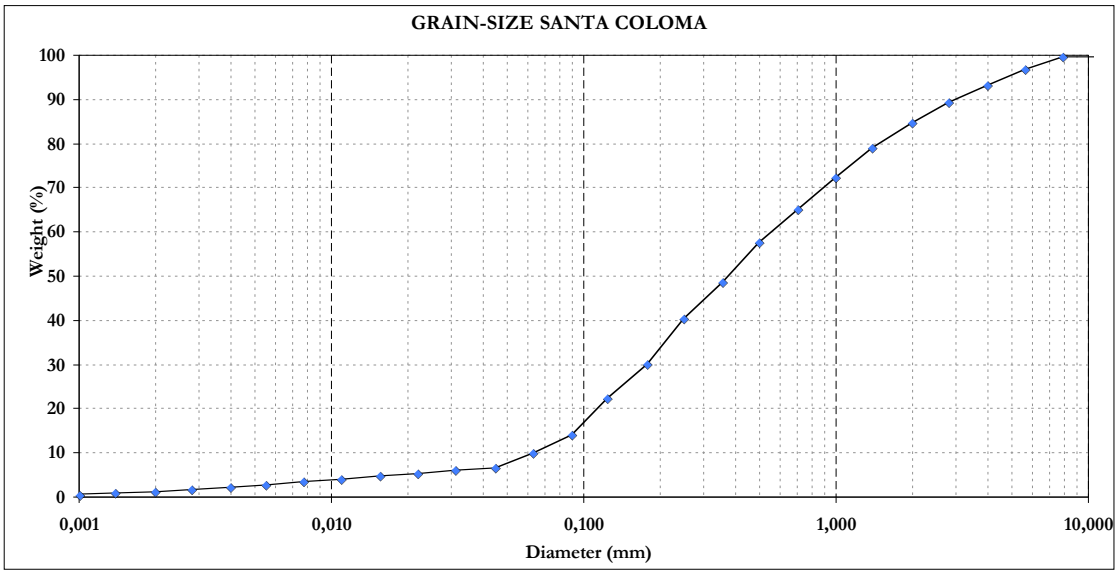

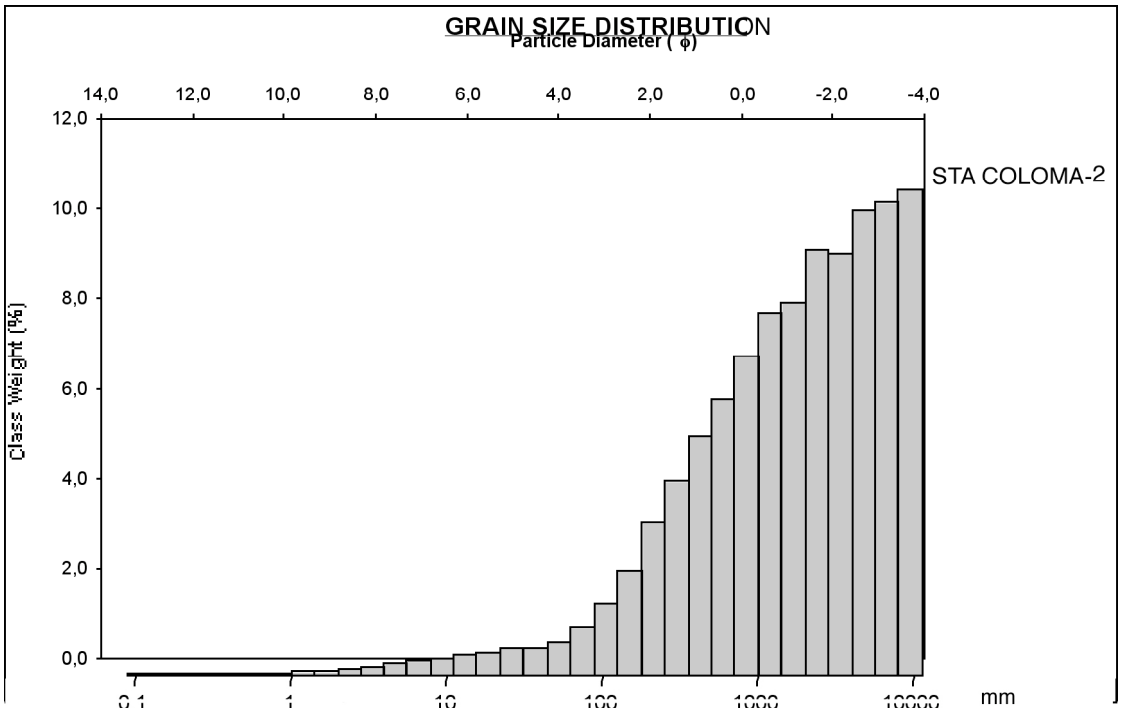

Fig. SM12 – On top, cumulative frequency curve of sample STACOLOMA-2. Santa Coloma terrace in the Valira Valley. Histogram: Sandy medium gravel or very fine gravel, poorly sorted, very fine skewed, platykurtic. Bimodal distribution for STACOLOMA-2 sample. Only for unimodal samples the sorting, skewness and kurtosis are therefore reliable.

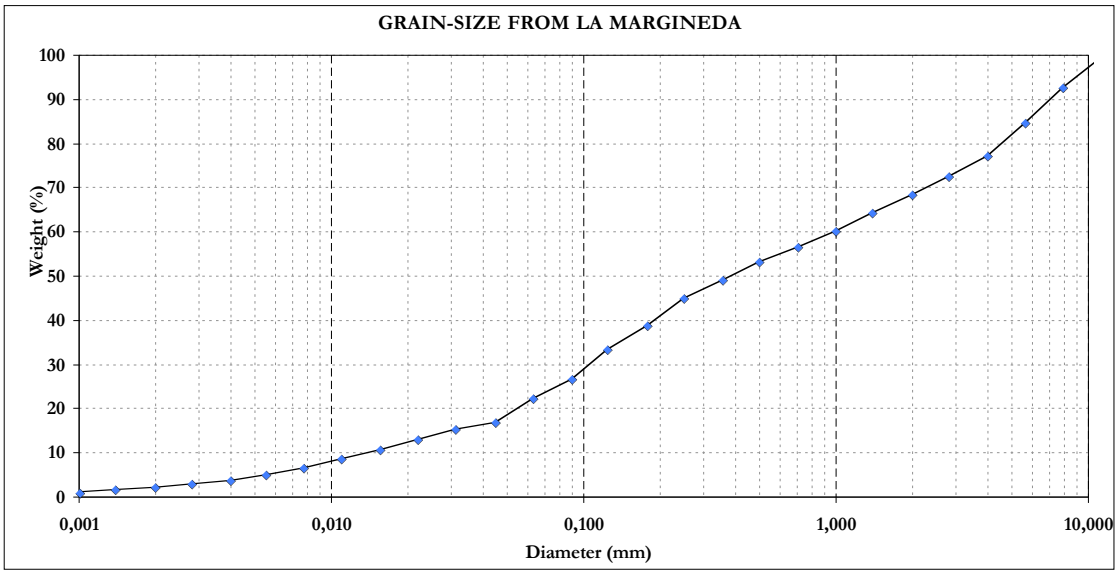

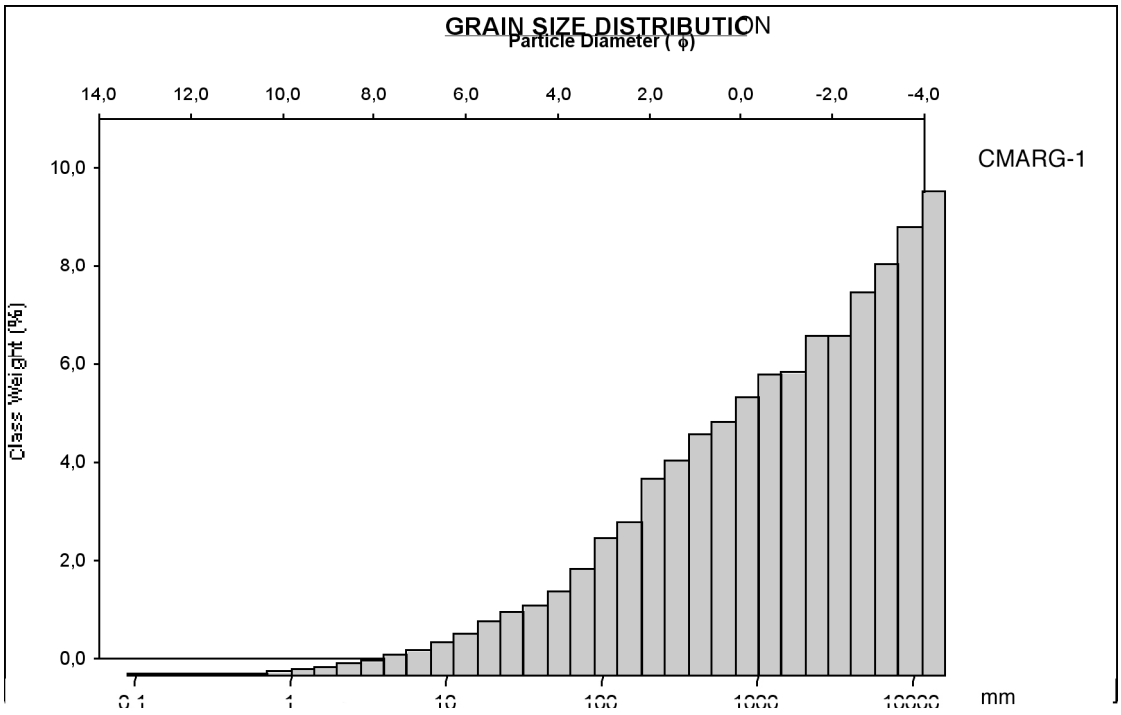

Fig. SM13 – On top, cumulative frequency curve of sample CMARG-1. La Margineda frontal moraine complex in the Valira Valley. Histogram: Muddy sandy gravel or very coarse silty sandy medium gravel, very poorly sorted, fine skewed, platykurtic. Unimodal distribution for CMARG-1 sample.

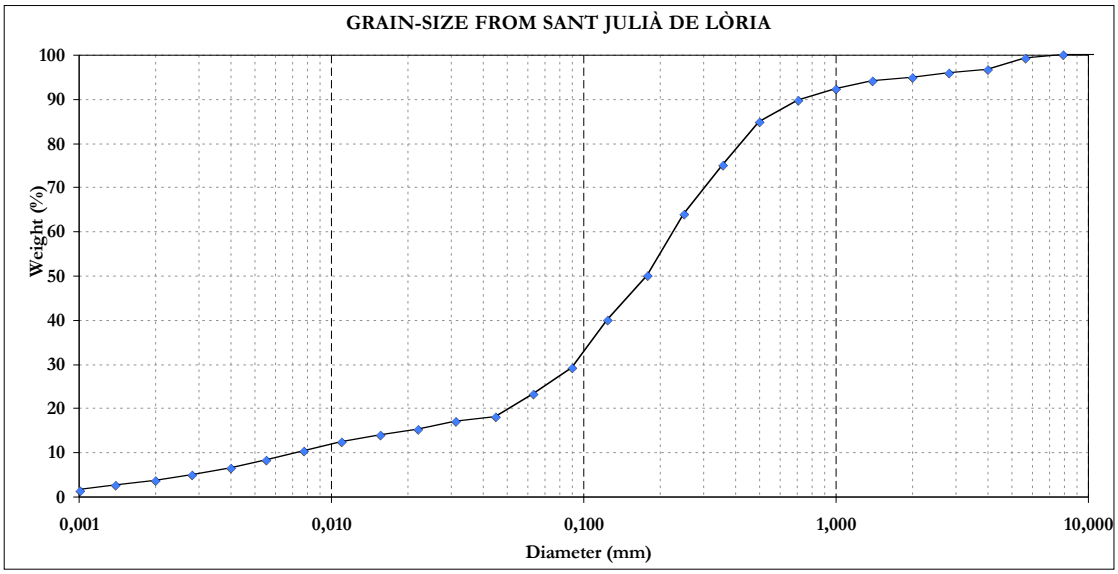

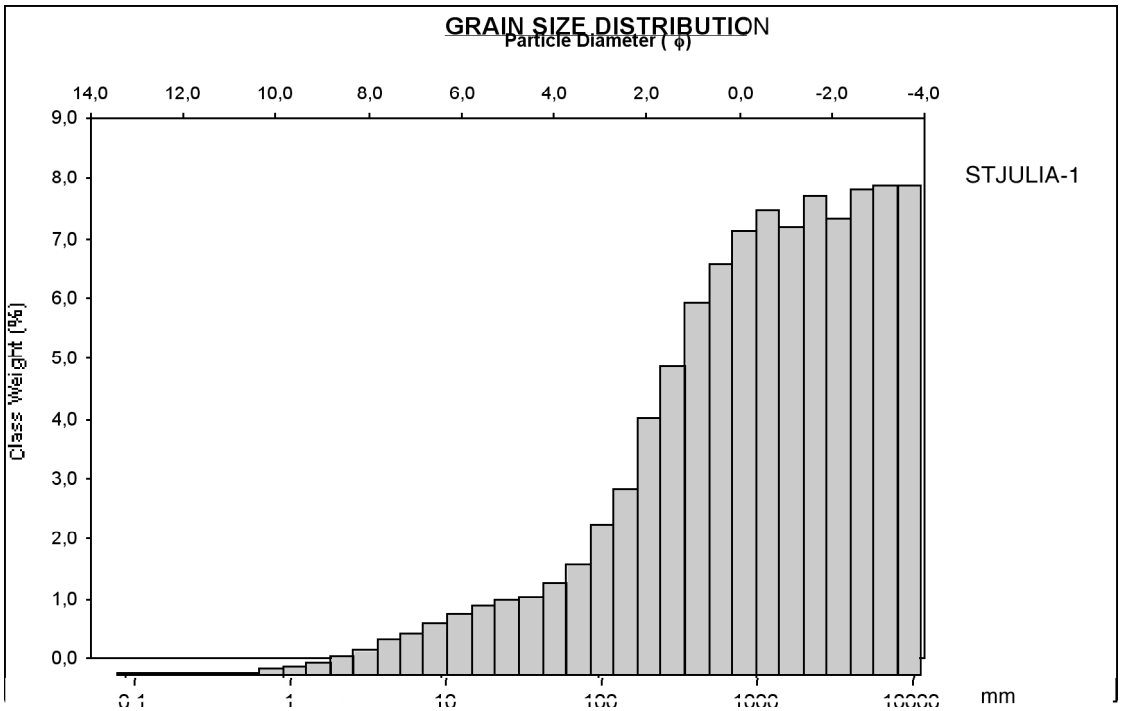

Fig. SM14 – On top, grain-Size from sample STJULIA-1. Sant Julià de Lòria (Valira Valley) glaciofluvial and moraine complex. Histogram: Muddy sandy gravel or very coarse silty sandy fine gravel, very poorly sorted, fine skewed, platykurtic. Trimodal distribution for STJULIA-1 sample. Only for unimodal samples the sorting, skewness and kurtosis are therefore reliable.

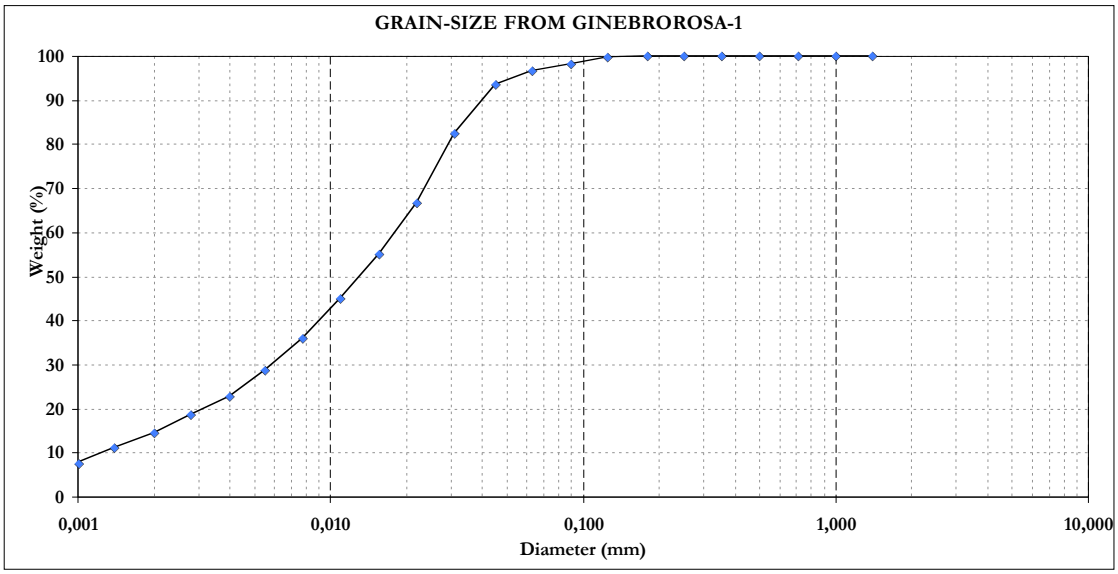

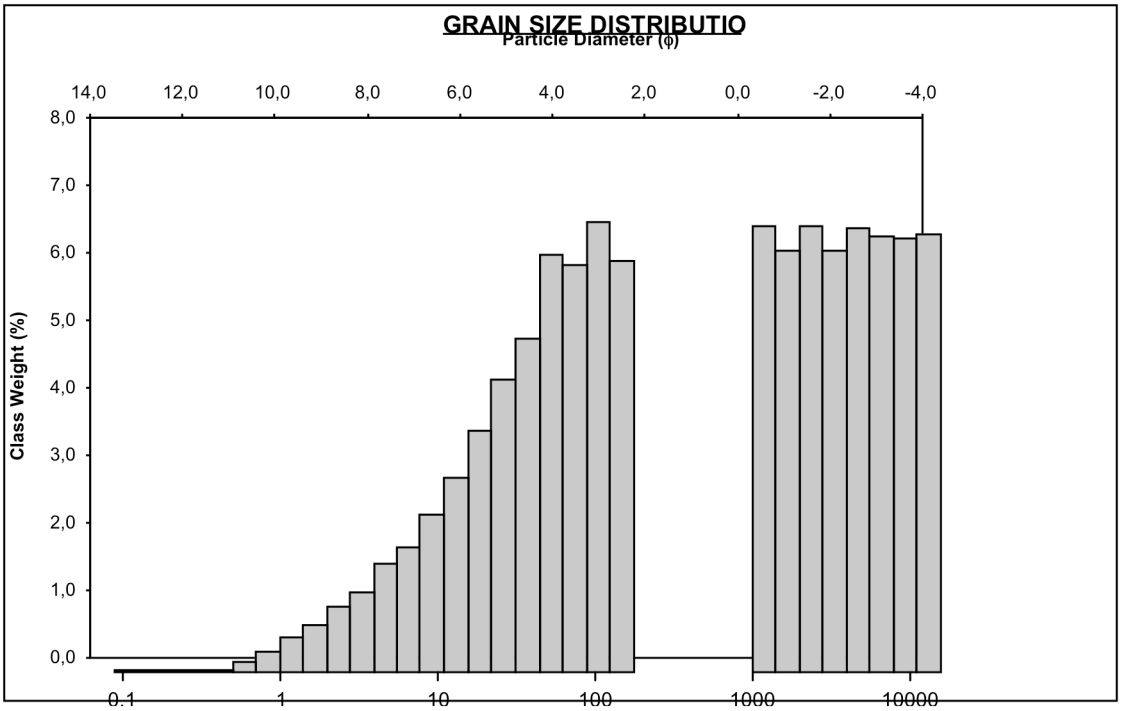

Fig. SM15 – On top, cumulative frequency curve of sample GINEBROSA-1 (Valira Nord valley). Kame terrace, glaciofluvial terrace and colluvium interdigitated. Histogram: Muddy sandy gravel or very coarse silty sandy medium gravel, very poorly sorted, very fine skewed, very platykurtic. Polymodal distribution for GINEBROSA-1 sample. Only for unimodal samples the sorting, skewness and kurtosis are therefore reliable.

2 POROSITY

Average effective porosity distribution of materials from the Principality of Andorra (**Fig. SM16**), whether lithological formations (the first ten items) or non-lithified sediments (the last eleven items) following the methodology of Plata and Rubio (2006). From a total of 106 measurements, it can be seen that, on porosity average, colluvium had the highest value, followed by glacio-fluvial terraces and sandy deposits. Non-lithified but consolidated materials, such as tills, have porosities similar to most bedrock formations. Bedrock formations had Cambrian and Ordovician age (Rabassa Conglomerate, Estana Fm., Seo Fm., Bar quartzite, Cava Fm., Ansobell Fm.; Hartevelt, 1970), Silurian slates (Poblet, 1990), Devonian schist (mainy impure limestones; Mey, 1965), granites mainly from the end of the Variscan orogeny (Jäger and Zwart, 1968), and faulting bands (mylonites) affecting both crystalline and metamorphic bedrock (Soler, 1990). Measures on sediments are for Holocene colluvium, scree, lacustrine, alluvial and sandy deposits, but also the upper Pleistocene (mostly glacially related deposits; Vilaplana, 1985), like glaciolacustrine and glaciofluvial sediments, tills (subglacial and supraglacial) or rock glaciers. Data from the Marcel Chevalier Earth Sciences Foundation: http://aquateca2.ddns.net/ (online August 2022).

Materials	e	n	W	DESVEST	Samples
Colluvium	0,38	27,68	13,76	12,34	12
Glacio-fluvial	0,29	22,74	10,59	10,11	23
Glaci-lacustrine	0,05	5,51	2,10	2,00	4
Rock glacier	0,20	16,75	7,23	7,61	15
Subglacial till	0,09	8,65	3,41	3,42	7
Supraglacial Till	0,18	15,76	6,73	4,45	8
Units	-	%	%	%	69

Table SM3 – Typical void ratio (e) values, porosity (n) and water content (w) from Andorran deposits (69 samples).

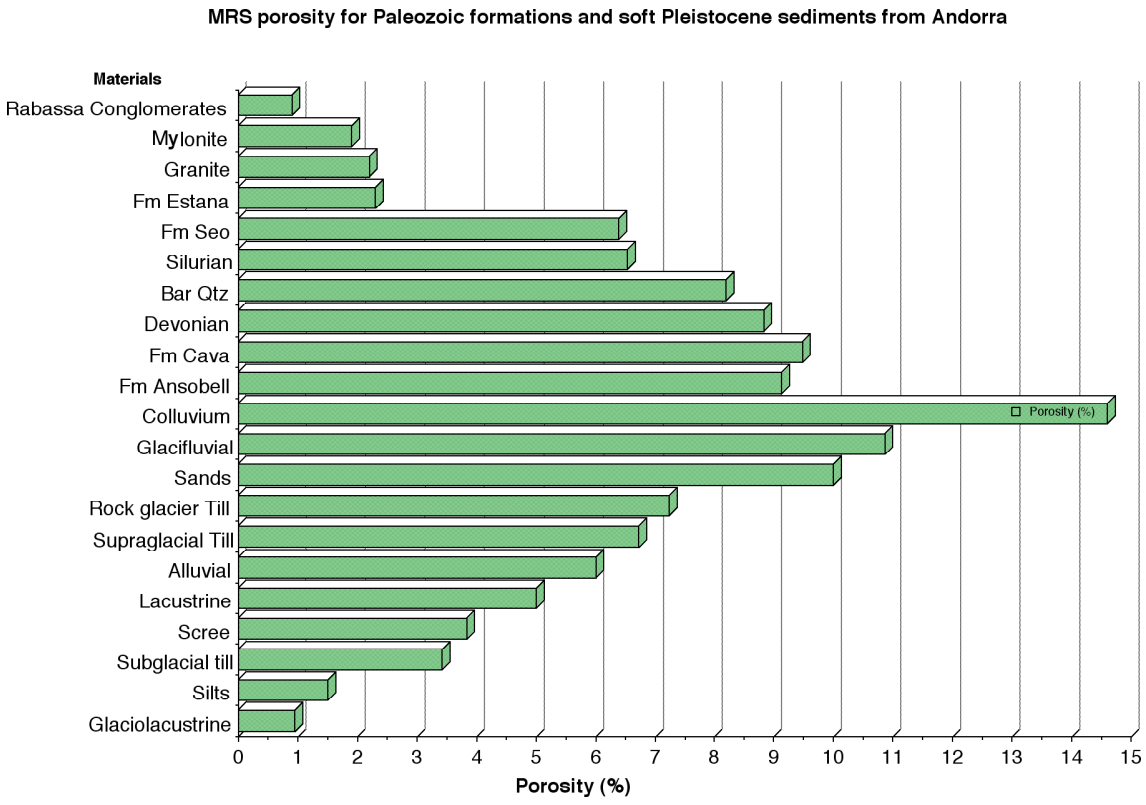

Fig. SM16: A porosity average of 5% for lithological data from the Principality of Andorra. Colluvium and glacio-fluvial deposits has the largest porosity (> 10%).

3 RADIOCARBON AMS METHOD

Carbon occurs in nature as three isotopes: ^{12}C, ^{13}C and ^{14}C. With the lowest atomic weight, ^{12}C is the most abundant (98.9%), while ^{14}C is rare (10^{-10}%; Walker, 2005). Carbon isotopes are incorporated into biological processes in equilibrium with their abundance in the natural environment. Biological processes, such as photosynthesis or the activities of some organisms, produce isotope fractionation. The measurement of the number of atoms of either isotope is obtained using a mass spectrometer. The standard ^{13}C / ^{12}C ratio is well known (δ ^{13}C‰). Most terrestrial samples have $\delta^{13}C$ negative values, whereas marine samples tend to have zero because their compositions are close to the standard (Pee Dee Belemnite, PDB; Walker, 2005). Measurement of ^{14}C activity and the isotope ratio ^{13}C /^{12}C used the Beta Analytic Inc. (Florida, USA) mass spectrometer facility and bulk organic fraction from sedimentary samples. Possible biological contaminants (i.e., fungi) were avoided by drying the samples immediately after sampling. After drying, the samples were isolated in aluminium foil, put into plastic bags, and stored at 4ºC in a dry and dark place before sending for dating. In the laboratory, organic matter was extracted using the ABA protocol (acid-base-acid washing (HCl-NaOH-HCl) to remove carbonates and possible humic acids). The resulting fraction was dried and prepared for dating.

4 LUMINISCENCE RESULTS

The data used to obtain the dose rate for each sample is listed in **Table SM4** , while OSL results are listed in **Table SM5**.

4.1 OSL DATES

NLL code	Field code	Gamma dose	1σ	Beta dose	1σ	U 238	1σ	Ra-226	1σ	Pb 210	1σ	Th 232	1σ	K 40	1σ	B.D.
122235	SANAV-0	1.310	0.024	2.324	0.034	30.957	2.983	25.962	0.353	3.993	33.940	44.666	0.473	723	12	5
122236	SANAV-1	1.867	0.027	2.729	0.038	26.694	3.841	29.026	0.387			84.658	0.747	781	13	125
122237	SANAV-2	1.499	0.029	2.741	0.049	29.319	5.154	29.913	0.540	50.775	59.582	47.858	0.659	879	17	1000
122238	VILALLER-1	1.077	0.029	1.488	0.039	36.946	6.903	32.278	0.615			45.645	0.755	355	9	250
122239	VILALLER-2	0.361	0.011	0.623	0.022	3.773	3.913	10.608	0.335	41.167	59.134	10.682	0.372	197	6	50
122240	UR-1	1.867	0.040	2.925	0.051	43.889	6.649	44.412	0.664			72.13	0.88	834	15	2000
122241	SORT-1	1.659	0.042	2.731	0.044	47.211	3.759	47.091	0.547	35.301	41.838	56.772	0.589	785	14	1700
122242	STA.COLOMA-2	1.340	0.029	2.685	0.036	49.405	6.958	32.273	0.612			32.519	0.567	929	14	200
122243	CMARG-4	2.017	0.008	3.180	0.021	50.537	2.714	54.105	0.488	49.980	3.256	68.889	0.387	937	7	1000
122244	STJULIA-2	1.943	0.046	3.071	0.051	56.875	5.769	52.361	0.643			72.183	0.800	855	15	150
122245	SEGUDET-1	1.447	0.039	2.065	0.037	38.619	4.075	44.627	0.524	6.367	57.688	57.562	0.638	530	10	600
122246	FAUCELLES-1	2.265	0.043	3.510	0.050	55.229	5.225	47.888	0.587			78.520	0.792	973	16	2800
122247	ARALL-4	1.927	0.044	3.006	0.050	45.227	5.730	49.941	0.604			72.823	0.776	851	15	275
122248	STPCodinet-1	1.362	0.029	2.368	0.044	34.748	5.735	31.318	0.539	13.822	83.956	45.958	0.695	720	14	5
122256	GINEBROSA-1	1.131	0.006	1.725	0.017	22.008	2.208	21.827	0.298	22.937	2.646	45.574	0.324	513	1	600
Units		**Gy kg^{-1}**				**Bq Kg^{-1}**										**cm**

Table SM4 – Dose of gamma and beta radiations, radionuclide activities (238U, 226Ra, 232Th and 40K) and burial depth (B.D.).

NLL no.	Name	Latitude	Longitude	a.r.b.	a.s.l.	Depth	Grain size	Age (ka)	Protocol	Dose (Gy)	n	Dose rate (Gy/ka)	w%
12 22 35	SANAV-0	N42º 23'20''	E1º 50'53''	+0 m	1045 m	0.05 m	Very coarse S.	**0.45 ± 0.05**	Quartz-OSL	1:34 ± 0.14	21	3.00 ± 0.11	15
12 22 35	SANAV-0	N42º 23'20''	E1º 50'53''	+0 m	1045 m	0.05 m	Very coarse sand.	**14.2 ± 1.3**	pIRIR290	56 ± 5	12	3.91 ± 0.12	15
12 22 36	SANAV-1	N42º 22'49''	E1º 50'55''	+38 m	1080 m	1.25 m	Fine sand	>69 n/a	Quartz-OSL	>250 ± n/a	1	3.63 ± 0.13	10
12 22 36	SANAV-1	N42º 22'49''	E1º 50'55''	+38 m	1080 m	1.25 m	Fine sand	**>180**	pIRIR290	>800	6	4.52 ± 0.14	10
12 22 37	SANAV-2	N42º 22'49''	E1º 50'55''	+29 m	1075 m	10 m	Medium lam. sand	>77	Quartz-OSL	>250 ± n/a	1	3.25 ± 0.12	9
12 22 37	SANAV-2	N42º 22'49''	E1º 50'55''	+29 m	1075 m	10 m	Medium lam. sand	**>200**	pIRIR290	>800 ± n/a	11	4.11 ± 0.13	9
12 22 38	VILALLER-1	N42º 29'04''	E0º 43'03''	+10 m	972 m	2.5 m	Coarse sand	**15.7 ± 1.2**	Quartz-OSL	40 ± 2	27	2.53 ± 0,12	5
12 22 39	VILALLER-2	N42º 29'04''	E0º 43'03''	+12 m	974 m	0.5 m	Coarse sand	**73.9 ± 4.5**	Quartz-OSL	>83 ± 3	37	1.13 ± 0.05	5
12 22 40	UR-1	N42º 27'30''	E1º 56'12''	+40 m	1226 m	20 m	Coarse sand	**103 ± 13**	pIRIR290	543 ± 62	10	5.30 ± 00.21	5
12 22 41	SORT-1	N42º 24'21''	E1º 07'45''	+35 m	700 m	17 m	Medium sand	>49 ± n/a	Quartz-OSL	>200	3	4.08 ± 0.19	5
12 22 41	SORT-1	N42º 24'21''	E1º 07'45''	+35 m	700 m	17 m	Medium sand	**>162**	pIRIR290	>800	3	4.94 ± 20	5
12 22 42	STA.COLOMA2	N42º 29'43''	E1º 29'56''	+15 m	975 m	2 m	Coarse-med. sand	**11.4 ± 1.4**	Quartz	44 ± 5	16	3.86 ± 0.17	5
12 22 43	CMARG-4	N42º 20'24''	E1º 28'13''	+65 m	990 m	10 m	Medium lam. sand	**91 ± 9**	pIRIR290	519 ± 48	10	5.72 ± 0.22	5
12 22 44	STJULIA-2	N42º 20'24''	E01º 29'20''	+20 m	890 m	1.5 m	Fine sand	**36 ± 3**	pIRIR290	205 ± 16	9	5.67 ± 0.22	5
12 22 45	SEGUDET-1	N42º 33'35''	E01º 32'20''	200 m	1500 m	6 m	Lam. fine sand	**141 ± 16**	pIRIR290	592 ± 62	17	4.20 ± 0.16	4
12 22 46	FAUCELLES-1	N42º27'17''	E01º29'57''	+10 m	1131 m	28 m	Bioturbated silt	**0.81 ± 0.05**	Quartz	4.32 ± 0.12	33	5.34 ± 0.25	5
12 22 47	ADRALL-4	N42º 19'43''	E01º 23'27''	+35 m	625 m	2.8 m	Medium lam. sand	**179 ± 15**	pIRIR290	843 ± 62	22	4.70 ± 0.15	5
12 22 48	STPCodinet-1	N42º 18'23''	E01º21'55''	+0 m	593 m	0.05 m	Medium sand	**0.19 ± 0.03**	Quartz	0.59 ± 0.09	27	3.08 ± 0.11	15
12 22 56	GINEBROSA-1	N42º 33'14"	E1º30'54.46"	200 m	1449 m	6 m	Laminated silt	**42 ± 8**	pIRIR290	151 ± 30	18	3.63 ± 0.13	5

Table SM5 – Global position of the samples. Optical Stimulated Luminescence (OSL) dating results obtained by the Nordic Laboratory for Luminescence Dating (NLL). Notes: a.r.b. – above river bed; a.s.l. – above mean sea level. (W) Estimated average water content used for dose-rate calculations of the luminescence dating ages.

4.2 TL DATES

Global position of the samples and results.

ITN no.	Name	Latitude	Longitude	a.r.b.	a.s.l.	Depth	Grain size	Age (ka)	Dose (Gy)	Dose rate (Gy/ka)
LUM-24	ADRALL-1	N42º19'47.2''	E01º 22'54.6''	+145 m	735 m	4.0 m	Coarse sand	Too old	n/a ± n/a	n/a ± n/a
LUM-25	ADRALL-2	N42º19'44.7''	E01º 23'6.7''	+124 m	714 m	2.0 m	Coarse sand	Too old	n/a ± n/a	n/a ± n/a
LUM-26	ADRALL-3*	N42º19'43''	E01º 23'27''	+35 m	625 m	2.8 m	Medium lam. sand	120 ± 5.5	1490 ± 39	12.417 ± 0.33
LUM-27	Cal Tolse*	N42º26'50''	E01º28'59''	+85 m	964 m	3.0 m	Coarse sand	125 ± 14	1552 ± 144	12.416 ± 0.36
LUM-272	Pont Trencat	N42º24'16''	E01º28'0''	+15 m	800 m	3.0 m	Laminated silt	0.55 ± 0.03	6.51 ± 0.2	11.836 ± 0.34
LUM-273	STJULIA-1	N42º 20'24''	E01º 29'20''	+20 m	890 m	1.5 m	Fine sand	32.8 ± 1.2	384.7 ± 6.2	11.728 ± 0.34
LUM-274	STA.COLOMA	N42º 29'43''	E1º 29'56''	+15 m	975 m	2.0 m	Coarse sand	9.5 ± 0.3	116.8 ± 1.5	12.294 ± 0.34

* Minimum ages

Table SM5 – Thermo-luminescence (TL) finite ages from the studied deposits: LUM-24 to LUM-27 from Turu and Peña-Monné (2006); LUM-272 from Gascon and Turu (2011); LUM-273 and LUM-274 by Jalut and Turu (2008). a.r.b. – above river bed; a.s.l. – above mean sea level.

5 OFFSET AND SATURATION

Differences between Quartz and K-Felspars exist. K-Felspars crystals are 1.43 times older than the Quartz ages (**Fig. SM17**).

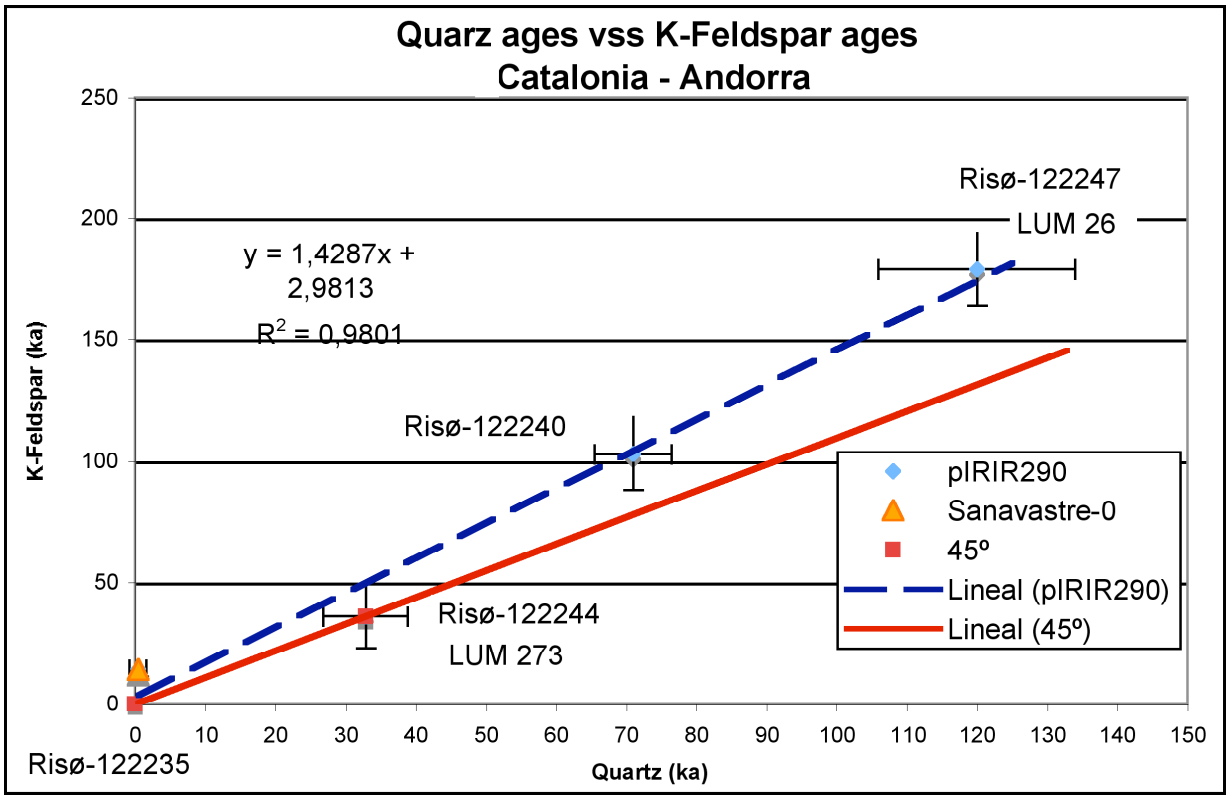

Figure SM17: Quartz versus K-Feldspar ages. Only available data pair are plotted from **Table SM5** (Risø or NLL laboratory) and **Table SM6** (ITN Sacavem laboratory). LUM-26 and LUM-27 are both from different sites but related to the similar weathered glaciofluvial terrace from Turu & Peña-Monné (2006), Turu *et al*. (2007) and Peña-Monné *et al*. (2011). Luminescence quartz ages for samples older than 30 ka a linear correction should be applied.

5.1 K-FELDSPAR BLANCH

The major problem in the luminescence dating of glacial deposits whether or not the signal was fully reset at the deposition time. If this is not the cause, the apparent luminescence age will overestimate the real age of deposition. The most widely accepted approach to identify incomplete bleaching is to carry out measurements from the current bed-load or directly from the active riverbed, looking at single grains or aliquots containing very few grains emitting luminescence signals. The level of residual doses is indirectly related to the transport energy (reflected by the grain size distribution, **Table SM1**) but also by the duration of light exposure and the light intensity. The latter is influenced by the direct light level (full sun or overcast sky) and, in particular, the turbidity of water. for Quartz determinations, the offset is < 0.5 ka (SANAV-0 and STPCodinet-1; **Table SM5**), a highly effective procedure for such a sedimentary setting. However, the applied pIR-IRSL 290 approaches have proven to have an offset of ≈ 14 ka (sample SANAV-0, **Table SM5**); nevertheless, in our study context, this offset is unacceptable (>20%) for samples older than 70 ka and acceptable for the oldest samples. Although doubling the samples for each dated level and measuring both signals (Quartz and K-Feldspar) or combining TL and OSL pIR-IRSL 290 we quote the offset range.

5.2 QUARTZ LATTICE SATURATION AND OFFSET

Following results from **Figure SM18**, K-Feldspar age inherence is higher than for Quartz samples below 25 ka since NLL-122244 (K-Feldspar age) and LUM 273 (Qtz age) are quite similar. Divergences between NLL-122247 (K-Feldspar age) and LUM-26 (**Figure SM18**) are related to the progressive quartz lattice saturation, not by K-Feldspar inherence. The divergence starting point is posterior to VILALLER-2 (NLL-122239) sample since Quartz measurements are compatible with finite ages. Adding to **Figure SM18**, the VILALLER-2 sample results, supposing that the mean Quartz and K-Feldspar age is the same and the 10% standard deviation since this is for the rest of the known K-Feldspar finite ages (**Table SM5**). Once the Quartz-KFeldspar relationship is known, age approximations can be estimated for samples older than 70 ka (**Figure SM19**). The main conclusion is that the low range of K-Feldspars ages stays inside the Quartz age ranges, almost for dates younger than the ADRALL-3 sample. For older Quartz ages than ADRALL-3, like Cal Tolse sample (LUM-27, **Table SM6**), a mean K-Feldspar age of 196 ka is expected following the relationships from **Figure SM19**; however, a wide range is also presumed (137 ka to 276 ka) for Cal Tolse met-out-till.

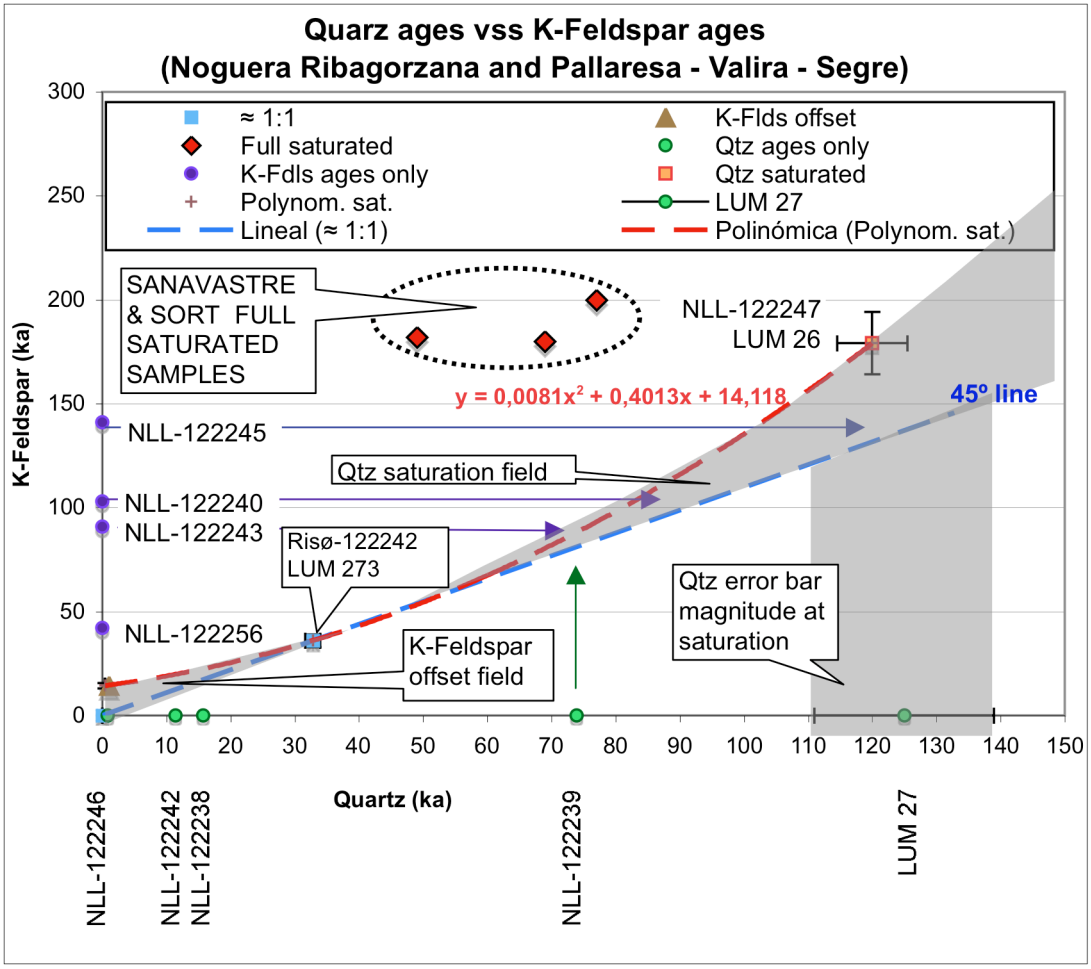

Figure SM18 – Quartz versus K-Feldspar ages from **Table SM5** and **Table SM6**. Quartz and K-Feldspar inheretance field is known from NLL-122246 sample. Unsaturated luminescence ages might follow the 45º line, while saturated luminescence ages are above the 1:1 line. Since a progressive amount of saturated quartz grains grow regarding their buried age, the path from LUM-26 to LUM-27 should be a continuous function until its full saturation. A random behaviour between both Quartz and K-Feldspar ages is then expected. The last is for Sort (NLL-122241) and Sanavastre (NLL-122236 and NLL-122237) samples, and the conclusion is that Quartz and K-Feldspar grains are both fully saturated.

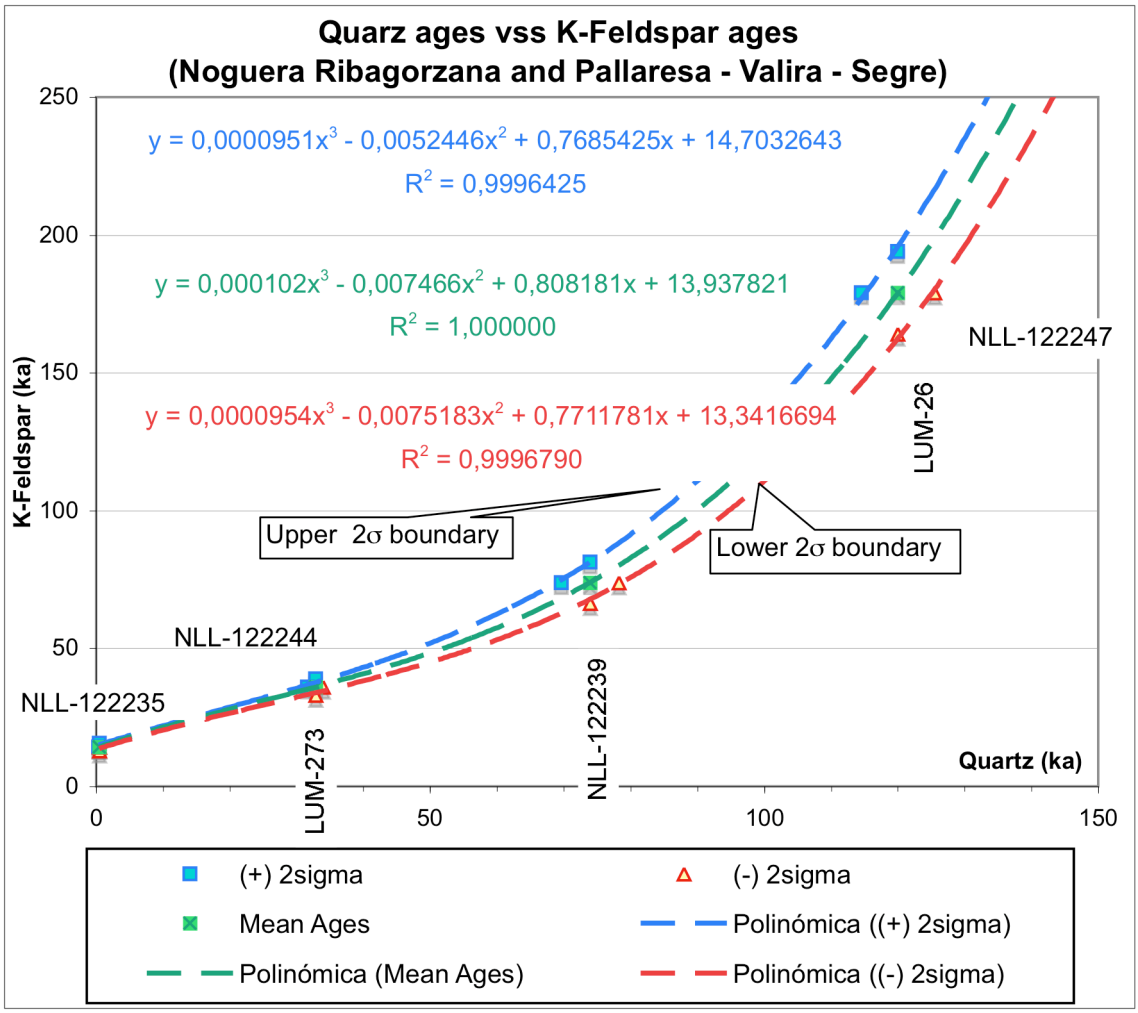

Figure SM19 – The best fit is determined by minimizing the difference between the K-Feldspar IPRIR290 age and the Quarz age from the TL at those samples with both data. For a few pairs of ages (K-Feldspar and Quartz), the range of fit is estimated using Pearson's correlation by using a continuous function. To consider the different uncertainty levels within the range of the ages from the pair of dated samples of SANAV-0, STJULIA-1, STJULIA-2, ADRALL-3 and ADRALL-4 (**Tables SM5** and **SM6**), a family of proper functions reports the best-fit solution using polynomial regressions. Each best-fitting function yields a quadruplet of solutions, and their differences regarding their mean value report about the two sigma's error bars.

6 FIELD DESCRIPTIONS

6.1 SANAVASTRE

At the southern part of the Cerdagne basin, close to the end of la Molina alluvial fan and at its eastern side, a weathered alluvial deposit of 7 to 8 m thick comprising schist clasts can be found, hanged about 20-35 m in the Escadarchs cone (**Fig. SM20**). On the western side of the la Molina, the alluvial fan calcareous cobbles and calck-shists pebbles are more abundant towards Prat village. The existent cuts in Sanavastre and Parts quarries confirm the upward catchment of these cones, but the same pedogenetical evolution is found for Escadarch and Sanavastre-Prats alluvial fan cones (Calvet, 1996). On the other hand, towards Sanavastre and Prats, a large fluvial layer is ten meters thick on the Segre River's left side (south). This fluvial bed (Mala Mort level) is hung about forty meters over the Segre River bed (Calvet, 1998). It comprises a layer with cross-stratification, presenting large cobbled lenses scattery cut by sandbanks: in the French Cerdagne, it shows weathering, totally decarbonated despite the southern Devonian calcareous contributions from the Tossa d'Alp massif (Poch et al., 2013). The Sanavastre fluvial terrace doubles downstream in a couple of weathered levels. Geopetal carbonation structures, carbonate nodules, and small clay accumulation are signalled by Poch *et al.* (2013) and arenized granites, however, rich-iron minerals remain unweathered (Calvet, 1996). On top, colluvium seals both levels. However, traces of periglacial dynamics, capping and solifuction features could be identified in Sanavastre (Calvet, 1996). A large solifluction lense reworked the higher Sanavastre level, already affected by decarbonatation (the capping is affected by worm pipes fill with carbonates, common in a posterior browning process), more even than the youngers colluvial deposits on the top (Calvet, 1996). Two samples were taken in the Abellorols lignite quarry at Sanavastre, one sample from each terrace sub-level; unfortunately, both are saturated, and only minimum ages of 180-200 ka are available (SANAV-1 and SANAV-2, **Fig. SM20**).

The sample SANAV-0 was taken 35 m downhill from samples SANAV-1 and SANAV-2, at the Segre's undisturbed riverbed. Since water saturation is complete on the riverbed, we suppose the highest water content for a porous media in or geological context (**Table SM3**).

Fig. SM20 – Sampling for OSL dating, from the Sanavastre fluvial terrace (Spanish Cerdagne) during 2012, with Dr. Marc Calvet. A) Sampling at the lower deposits (SANAV-2). B) Sampling at the top deposits (SANAV-1).

6.2 VILALLER

The Quaternary sedimentary record of this valley was studied by Vilaplana (1983a, 1983b), Vilaplana *et al*. (1989), Vilaplana and Bordonau (1989) and Bordonau (1992). These authors recognise two main sedimentary units, a non-deformed glaciofluvial unit and a deformed unit (**Fig. SM21**). The deformed unit's laminated sandy lenses are embedded in a matrix-supported diamicton, interpreted as a melt-out till (**Fig. SM22**). From the convergence with the Noguera de Tor and the Noguera Ribagorzana valleys, several kilometres south of Vilaller, a few terrace remnants at ca 15–20 m above the present-day talweg were recognized by Vilaplana (1983a), interpreted as glacio-fluvial nature (Vilaplana, 1983a,1983b) and without contact with glacial sediments outside from Sant Mamés. This site is less than a half kilometre south of the Seminari de Vilaller frontal moraine (Vilaplana, 1983a, 1983b; Bordonau *et al*., 1989; Bordonau, 1992; Pallàs *et al*., 2006). A thick sedimentary infill exists behind the Seminari de Vilaller (Bordonau, 1992), containing diamicton to glacio-lacustrine rhythmites at the bottom of the sequence. The bottom-set is overlapped by coarse grain deposits, from foresets to a topset, in a general shallowing sequence evolution (Bordonau, 1992). The Seminari de Vilaller topset is located at the same absolute height as the Sant Mamés glacio-fluvial unit (see figure IV-3 from Bordonau, 1992; original from Vilaplana, 1983a and reproduced in **Figure 5** from the main text).

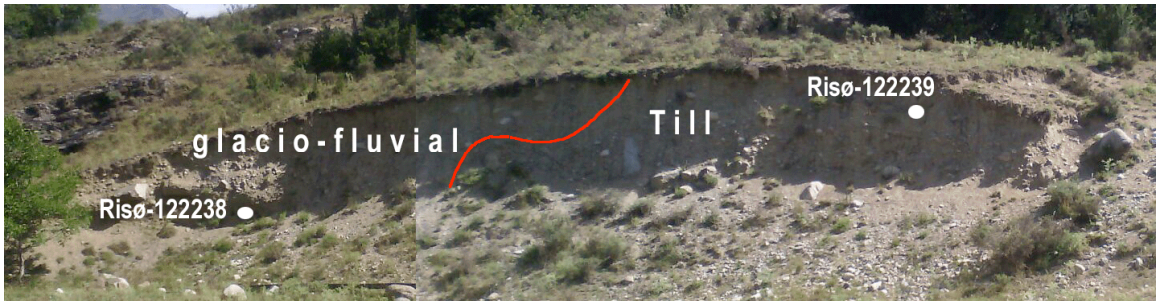

Fig. SM21 – Sketch-pad from the Sant Mamés outcrop, in which glaciofluvial deposits (122238; VILALLER-1; 15.7±1.2 ka) onlap glacial till (sample 122239; VILALLER-2; 73.9±4.5 ka). The onlap contact between both subunits (red line) is an unconformity.

Fig. SM22 – Sampling at the Sant Mamés outcrop (9th September 2011). A) To the left - eastern side of the outcrop - Diamicton on the lower zone of the outcrop and deformed rhythmites on the top, conform to the melt-out till deposits. B) To the right, western side of the outcrop - in which glacio-fluvial sedimentary deposits were sampled. On top, horizontal bedding with sands and gravels is crudely imbricated, indicating a high energy transport by water (that overlaps the melt-out-till). Beneath, horizontal bedding with big boulders embedded in a sandy gravel unit (type C facies of Krzyszkowki and Zieliñski, 2002) partially erodes the glacio-fluvial sampled unit.

6.3 UR

Two types of deposits can be distinguished in a restored area from the French N20 highway: a thick bed of rolled cobbles and imbricated gravels, with an ochre sandy matrix (**Fig. SM23**), attributed to the local terrace T4 (Calvet, 1998; Calvet *et al*., 2011). On top, a melt-out-till intensely weathered includes rinds surrounding clasts (Calvet, 1998). In continental environments, rinds may indicate a very long exposure period (Mahaney *et al*., 2014). Saple UR-1 was collected from the glaciofluvial unit. However, a gap between the two formations could exist since the elevation, and the paleocurrents from the imbricated pebbles can be related to the Rahur River.

Fig. SM23 – Sampling UR-1 (September 10th 2011), on a middle position of the Ur-Llaurar complex, glaciofluvial terrace from the Rahur River (French Cerdagne).

6.4 SORT

A former glacial front position is often deduced from the associated sedimentary deposits, such as the starting point of a glaciofluvial terrace, hanged glacial deposits and Kame terraces (Turu *et al*., 2011; Ventura and Turu, 2022). The SORT-1 sample was collected from a sandy layer from such outwash terrace (**Fig. SM24**).

Fig. SM24 – Sampling (9th September 2012) for OSL dating (SORT-1), from the Noguera Pallaresa fluvial terrace +40 (a.r.b.), at Sort. The deposits comprise medium sands showing planar lamination, following the type C facies of Krzyszkowki and Zieliński (2002); they are slightly tilted toward their former apex, which has now disappeared.

6.5 STA COLOMA

Bladé (1875) and Penck (1884) recognised that the ice invaded the central valley from Andorra close to Santa Coloma village (975 m a.s.l.). Chevalier (1906, 1907) located the terminal moraine of the main glacier of Andorra 29 km long, close to Santa Coloma (1030 m). Nussbaum (1956) also recognised this terminal moraine and indicated the presence of a fluvial terrace in a former quarry. Deposits show finning-upward sequences deposited from high-energy floodings (Turu and Peña-Monné, 2006). The first sampling for TL dating was done on 15th December 2005 (LUM-274, 9.5±0.3 ka, **Fig. SM25**), and the second sampling of the same sand bed but on a lower stratigraphic position was done on 11th September 2011 (STACOLOMA-2, Qtz-OSL, 11.4±1.4 ka, **Fig. SM25**).

Fig. SM25 – TL sample (LUM-274) taken with a large steel tube within a sand bed of the Santa Coloma fluvial terrace in March 2006 (picture from the left). The OSL sample for Santa Coloma fluvial terrace (STA.COLOMA-2; photo from the right, September 2011) was collected in a former open-pit quarry restoded in 2016. Only small portions of the outcrop still exists.

6.6 LA MARGINEDA

Southward from Andorra la Vella, the La Margineda site is surrounded by calcshists producing a narrower valley. Glaciofluvial clasts and sands, lithologically related to the granitic catchments from the main valley, conform to the terminal moraine complex from La Margineda (Panzer, 1926; Nussbaum, 1935; Llobet, 1947; Turu, 1994; Turu and Peña-Monné, 2006; Turu *et al*., 2007; Turu, 2011), located 50-60 m a.r.b. (**Fig. SM26**). For Nussbaum (1934) this place is where the Valira glacier reached its maximum extent. Llobet (1947) concluded that there were two glacial cycles in Andorra, corresponding to the Riss and Würm, and an older glaciation. This author concluded that La Margineda was the terminal moraine from the penultimate glaciation. However, Fontboté et al. (1957) doubted the glacial origin of the La Margineda deposits. Works to open a new road enabled Prat (1980) to reconsider these deposits as a recessional moraine. Posterior open-pit excavations permitted Turu (1994) to identify a kame terrace at +55 m beneath a thick scree deposit. Turu and Peña-Monné (2006) identified weathered moraine deposits attributed to the PGC (Turu et al., 2007). As described above, we were able to date the glacio-fluvial colluvium-kame terrace transition located +65–75 m a.r.b. as from the early Würm (CMARG-4, 91 ± 9 ka; MIS 5b-5c; Table 1). The Valira glacier subsequently partly eroded the MIS 5c alluvial fan deposits during a re-advance.

The current road cut outcrop includes a small portion of glaciofluvial deposits beneath colluvial sediments, mainly from local lithology (**Fig. SM27**). Both sedimentary facies (colluvial and glaciofluvial sediments) show strong compaction, which should be related to a glacier loading. A posterior glacier advance might be responsible for overconsolidated the aforesaid deposits. The age of those compacted scree (**Fig. SM28**) is from 22.29 ± 0.09 ka BP (ß-489299) or 26.566 ± 0.365 ka cal BP (δ13C = -23.1 ‰ organic fraction). However, the general glacier recession from La Margineda must be earlier than the deposit of very coarse scree from a rock avalanche (**Fig. SM29;** Tossal

Vinyalet) dated as 13.32 ± 0.04 ka BP (ß -489301; sample LM2b) or 16.018 ± 0.183 ka cal BP (δ13C = -24.7 ‰ organic fraction), and much older age is from the inorganic fraction (26.2 ± 0.1 ka BP; sample LM2a; ß-489300; δ13C = -6.3 ‰; δ18O = -5.8 ‰), which should be held a fraction of inactive carbon coming from the neighbouring basement (marine Devonian calcshists), and thus an invalid age for sample LM2a.

Southward from La Margineda, in Aixovall (**Fig. SM30**), an existing outcrop (16th February 2022), let us confirm where the glacier front was located when the Valira glacier consolidated unit 2 (**Fig. SM28**). We analyse the stratigraphy of this large outcrop (**Fig. SM30**), and we recognise the same layers as in La Margineda; however, unit 2 is here tilted and deformed. Unit 3 is also recognised by the CaCO3 cementations. The chronology of the sedimentary units in La Margineda and in Aixovall are assumed to be the same.

Fig. SM26 – Aerial view from La Margineda and Santa Coloma (to the north). This view illustrates how the bottom of the valley changes its width southward. The valley is narrower to the south of La Margineda. Cited sites are signalled in this figure, as well as the location of the dated samples.

Fig. SM27 – General overview of La Margineda outcrop. Consolidated colluviums, embedded granite cobbles. The rectangular area is exposed in **Fig. SM28**.

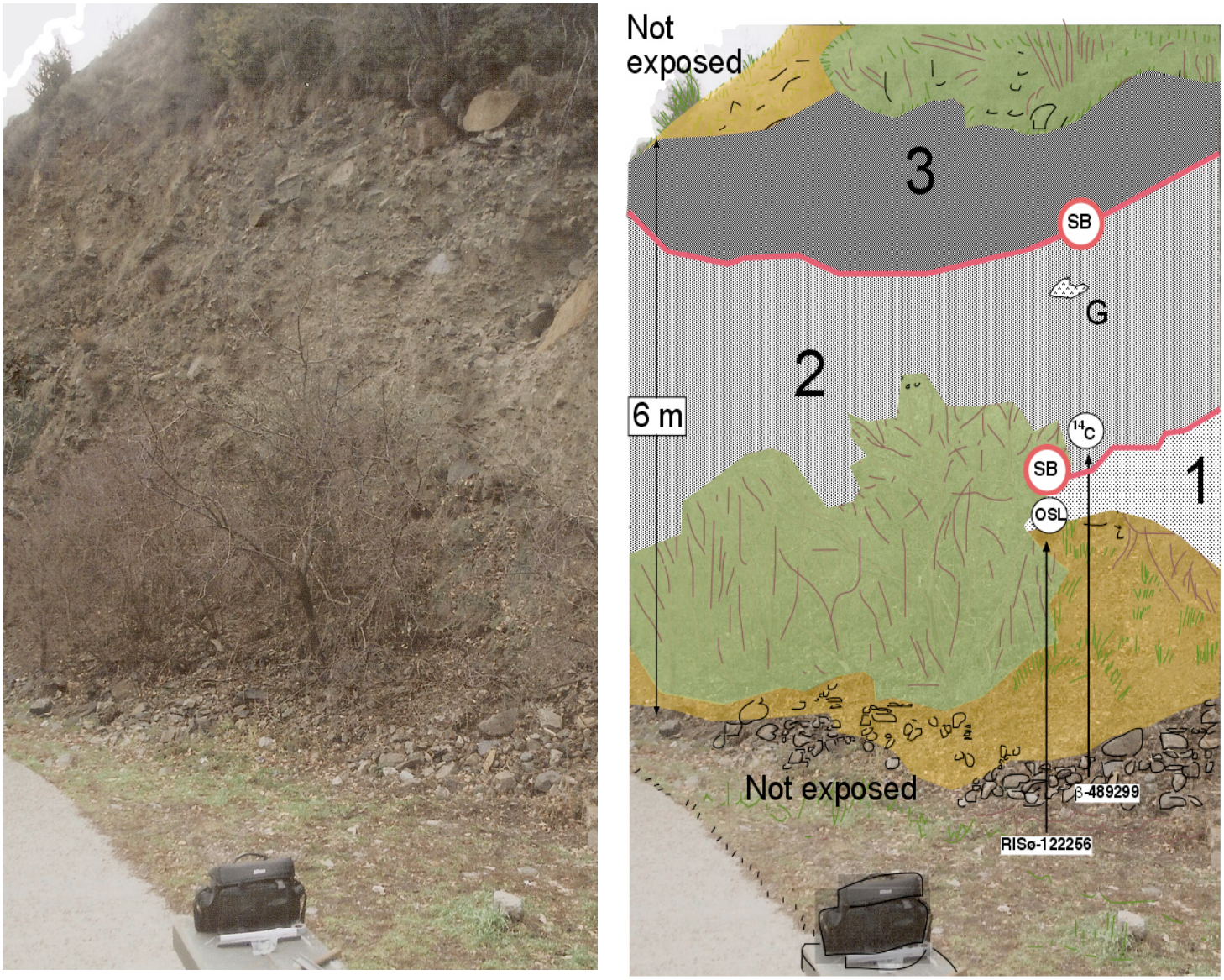

Fig. SM28 – Sedimentary units from La Margineda consolidated colluvium. Unit 1: Gravels and sands showing coarse crossbedding. Unit 2: Coarse to fine grain-size sequence (finning-upward) of colluvium. Unit 3: New finning-upward sequence in colluvium. G: granite. The boundaries between units are erosive surfaces. SB surface boundary (here, an erosive contact).

Fig. SM29 – Tossal (Vinyalet) exposure, 100 m southward from the previous one. Coarse scree deposits from an ancient rock avalanche at La Margineda (March 2018) were dated. This is not consolidated scree but partially cemented by carbonates that percolate through porous media from highly alkaline meteoric waters. Such carbonates may come from the dissolution of the neighbouring Devonian calcshists (on top of the picture).

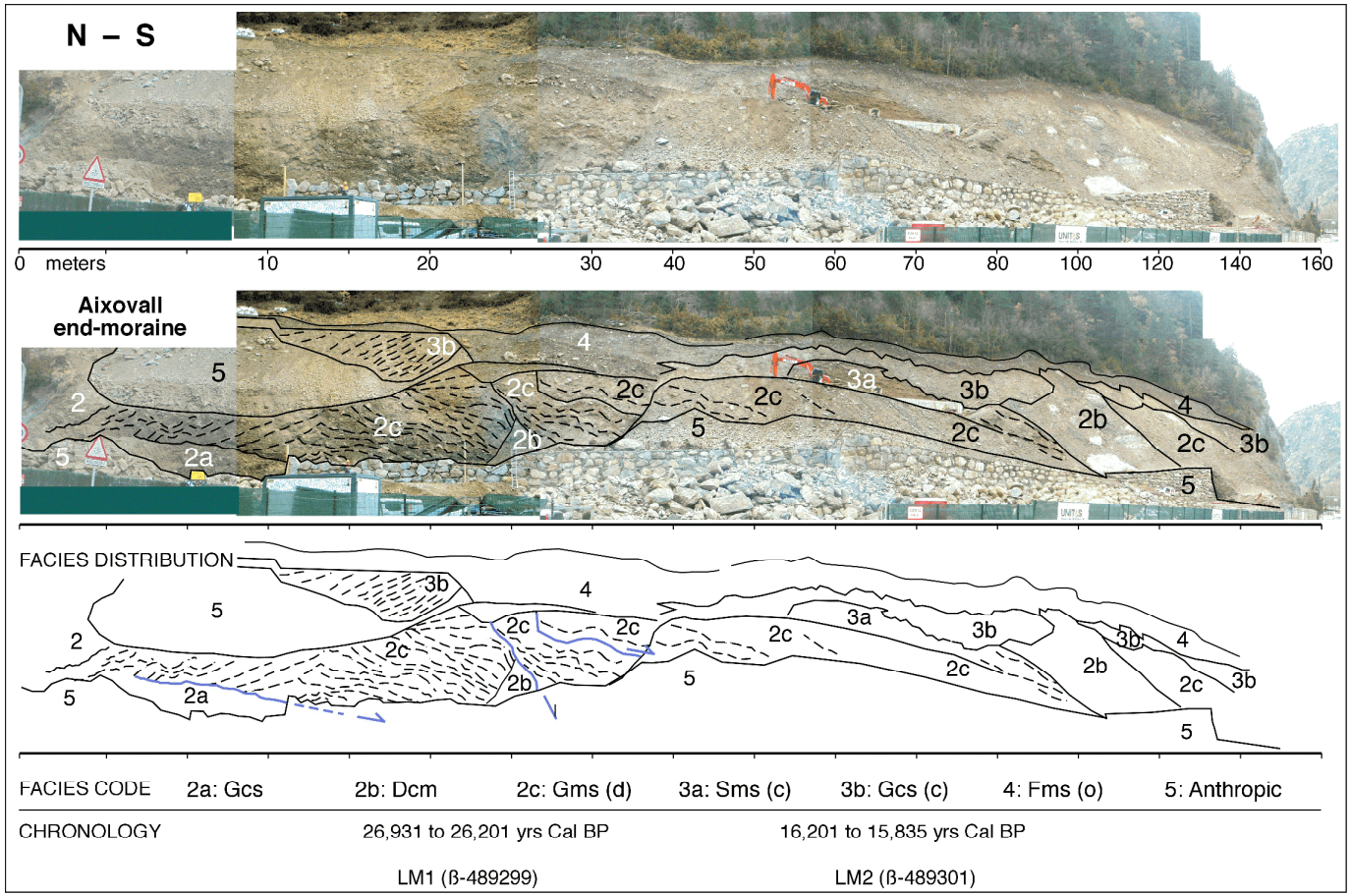

Fig. SM30 – The Aixovall outcrop from the MIS 2 La Margineda glacier front (16th february 2022). Unit 2a: Supraglacial till. Unit 2b: Deformed glacio-fluvial mixed with colluvium from the glacier motion in its front. Unit 2c: Similar to unit 2b but prevailing slope colluvium over the glacio-fluvial facies. Unit 3a: Fine grain-size slope sediments, including cemented CaCO3 levels. Unit 3b: coarse grain-size slope sediments, mostly CaCO3 cemented. Unit 4: Organic fine grain-size slope sediments and soil. Unit 5: Hand-made slopes and masonry walls.

6.7 ST JULIA

In south Andorra, Prat (1980) signalled erratic boulders on the left side of the valley in Sant Julià de Lòria. Not far from those erratics, Turu (2011) noted a supraglacial till that involves a melt-out till comprising cross-stratified sands, onlapping coarse colluvium lying over the basement. The cross-stratified sands were dated using TL (Jalut and Turu, 2008; **Fig. SM31** and **SM32**), while the melt-out till was dated using p-IRIR (NLL-122244; **Fig. SM33**).

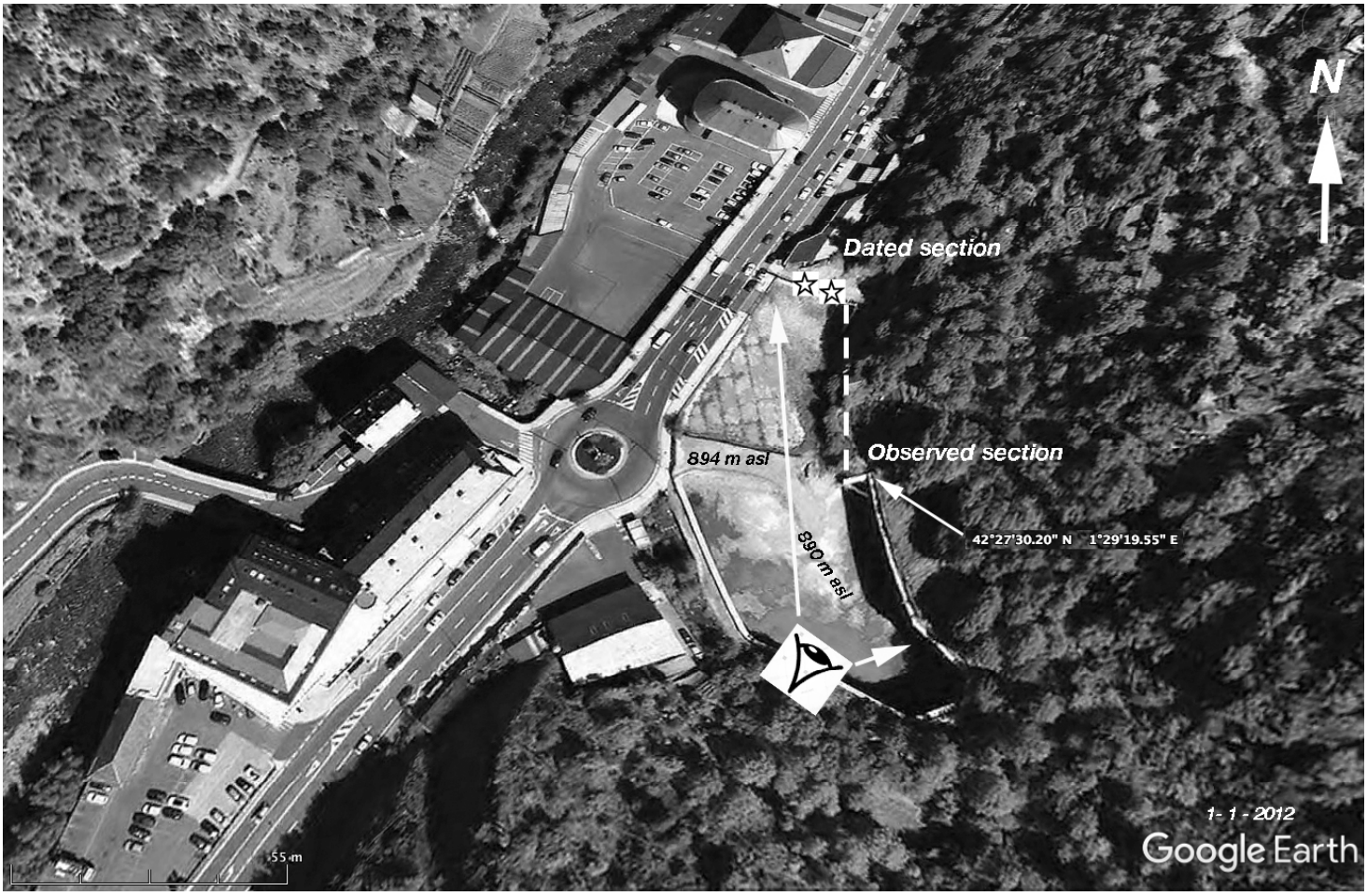

Fig. SM31 – Aerial picture from the south Sant Julià de Lòria area. Point of view (eye symbol) of an extensive open pit excavation from which sedimentary descriptions are. The position of the dated section is in the picture plotted as a star symbol.

Fig. SM32 – Exposure of slumped slope deposits' upper part that partially erode the melt-out till and the glaciofluvial sandy layer. From the same thin sand level, the TL sample LUM-273 (33 ka) was taken on the 16th of March 2006 and the OSL sample STJULIA-1 (36±3 ka) on 11th September 2011.

Fig. SM33 – Upper part of the Sant Julià de Lòria outcrop, laminated sands on the ablation-till. Sampling (STJULIA-1) was done just below the unconformable slope sediments.

When inspecting an open pit excavation in Sant Julià de Lòria, the deposits were formed by glacial erratics boulders accumulation, allowing for recognition of sharp facies changes, from glacio-fluvial gravels to colluvium both overlapping the boulders (**Fig. SM34**). A lodgement till and its correlative surface (an unconformity) divide the outcrop in two. Beneath this unconformity, classical facies changes between alluvial plain and colluvium are found. The evolution of the sedimentary sequence advocates for a recurrence of a narrower glacial front on top. Nevertheless, boulders are located mainly on the deposits laying over the lodgement till. Cross-stratified sands were dated using TL (**Fig. SM32**), and melt-out till sands were dated by using p-IRIR (**Fig. SM33**). Both sand layers had intact bedding, so we interpret that the coarse deposits and the cross-stratified sands were synchronous. Since both sediments interdigitate with fine colluvium, we interpret the whole deposit as part of a hummocky moraine within an ice-walled lake plain, the overall relative to a supraglacial land system (Johnson & Clayton, 2005). A stagnant ice void allows enough place for the sands to pile up at its melt. On top of the sequence, a discontinuity is identified (SB 1; **Fig. SM34**) between the deposits of boulders and post-glacial colluvium of unknown age.

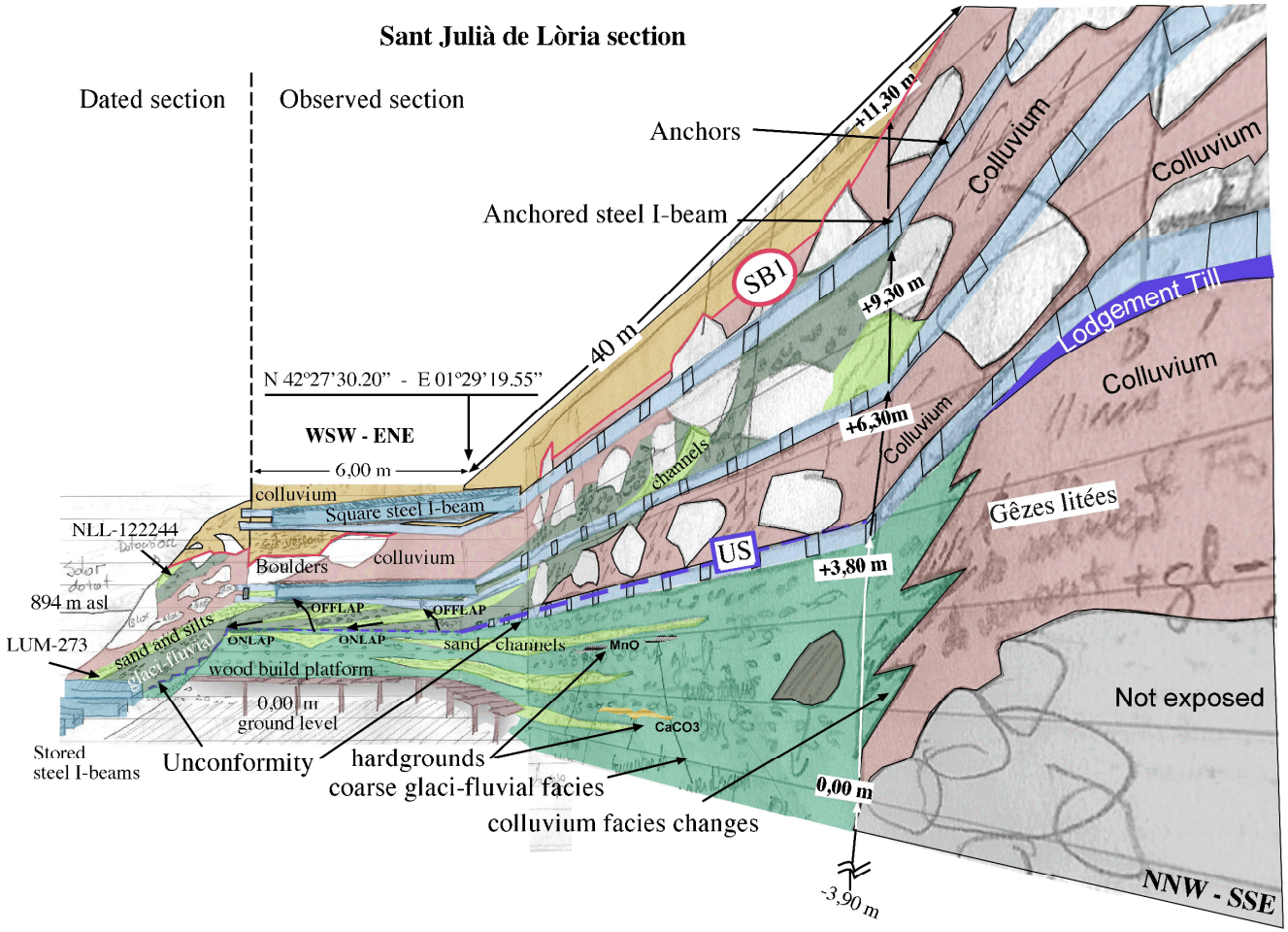

Fig. SM34 – Sketch of an open pit excavation 5 meters below the highway, south Sant Julià de Lòria (886 m a.s.l.), indicating the sandy layers dated (LUM273 and NLL-122244). The open pit is a 40 m long exposure of 16 m high. Solid blue lodgement till. Green colours: gravels – sands. Brown colours: colluvium. Line in red: discontinuity. Blue dotted line: unconformity. Grey: non-exposed section, covered by pied-up boulders. The lodgement till bisects the outcrop (and its correlative unconformity). Beneath this unconformity (US), thick fluvial gravels interdigitate with colluvium. Erratics are found only on top of the lodgement till and the unconformity. Such boulders are embedded in a gravely bedded matrix that interdigitates with fine colluvium. On top, colluvium progrades the sediments beneath the surface boundary 1 (SB1).

6.8 SEGUDET

Three generations of glacio-lacustrine and glaciofluvial deposits are present in Segudet (Turu et al., 2017). The highest one is in Redort (1530 m a.s.l.; Turu and Bordonau, 1997). A lower deposit is beyond the Creu de Nora gorge (1485 m a.s.l.; Turu and Bordonau, 1997), and the lowest glacio-lacustrine deposits are close to the Segudet vlillage (until, 1390 m a.s.l.; Vilaplana, 1985). The highest lacustrine rhythmites remain over a thick, gravely unit (outcrop IV-5.1.1 from Turu and Bordonau, 1997; http://llacglacial.ddns.net/). Some relicts of colluvium deposits had been observed at “Dame Coiffée”, including macrocharcoals remains (outcrop IV-5.1.9 from Turu and Bordonau, 1997; http://llacglacial.ddns.net/) which could indicate a non-glaciated period for its formation. Sample SEGUDET-1 was taken in a silty-clay laminated layer beneath the colluvium formation (**Fig. SM35**).

Outcrops (in Catalan, on line in August 2022)

outcrop IV-5.1.1 - http://www.mediafire.com/view/0s49akg6p6mjebe/Fitxa%20IV-5.1.1.pdf

outcrop IV-5.1.9 - http://www.mediafire.com/view/psrokf3pt60btbn/Fitxa%20IV-5.1.9.pdf

Fig. SM35 – The sample SEGUDET-1 was taken on the 11th of September 2011 from rhythmites of a former kame terrace complex and, on top, stratified colluvium (from the Eemian interglacial) in Segudet (NW Andorra).

6.9 FAUCELLES

South Sant Julià de Lòria, in a lateral torrent +140 m from the bottom of the valley, grey laminated silts over massive blue-grey sands were sampled for OSL dating (FAUCELLES-1; **Fig. SM36**) on the 11th of September, 2011. Damming in the lateral valley did occur since lacustrine silts and clays exist. However, the ice-damming hypothesis drawn by Turu et al. (2017) is completely discarded. Also, in the lower part of the Valira river, a former landslide obturates the Valira valley, and deposits of impure rhythmites sedimented at 532±32 years ago (TL dating, LUM-272; Gascon and Turu, 2011). We interpret that Faucelles sediments come from the erosion of the upper basin, where using the methodology of Farré (2000), high erosion vulnerability exists at 2600 m a.s.l. (**Fig. SM37**). In the Middle Ages (1.202±0.050 ka AD), local flooding may produce Faucelles' deposits, probably by the increase of erosion episodes in the upper part of the valley at that time.

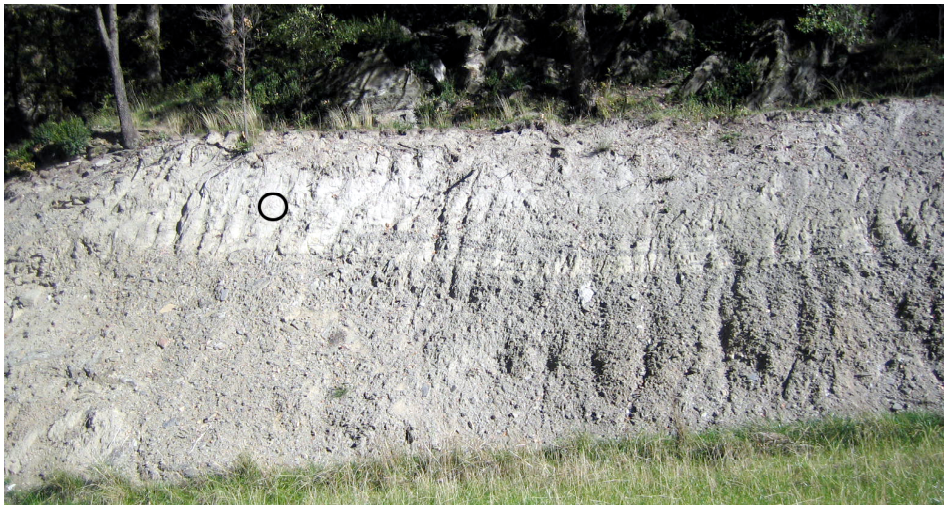

Fig. SM36 – Exposure showing the lower part of the deposit massive diamicton deposits comprising a bed of clasts from local lithology (metamorphic slates) interpreted as a debris flow. Laminated silts and sands predominate, being massive on top. We interpret this as a result of massive flooding in the narrow valley of the Auvinyà torrent (photography by Xavier Planas i Batlle). This exposure has a height of 4 m; the black circle indicates where the FAUCELLERS-1 OSL sample was collected.

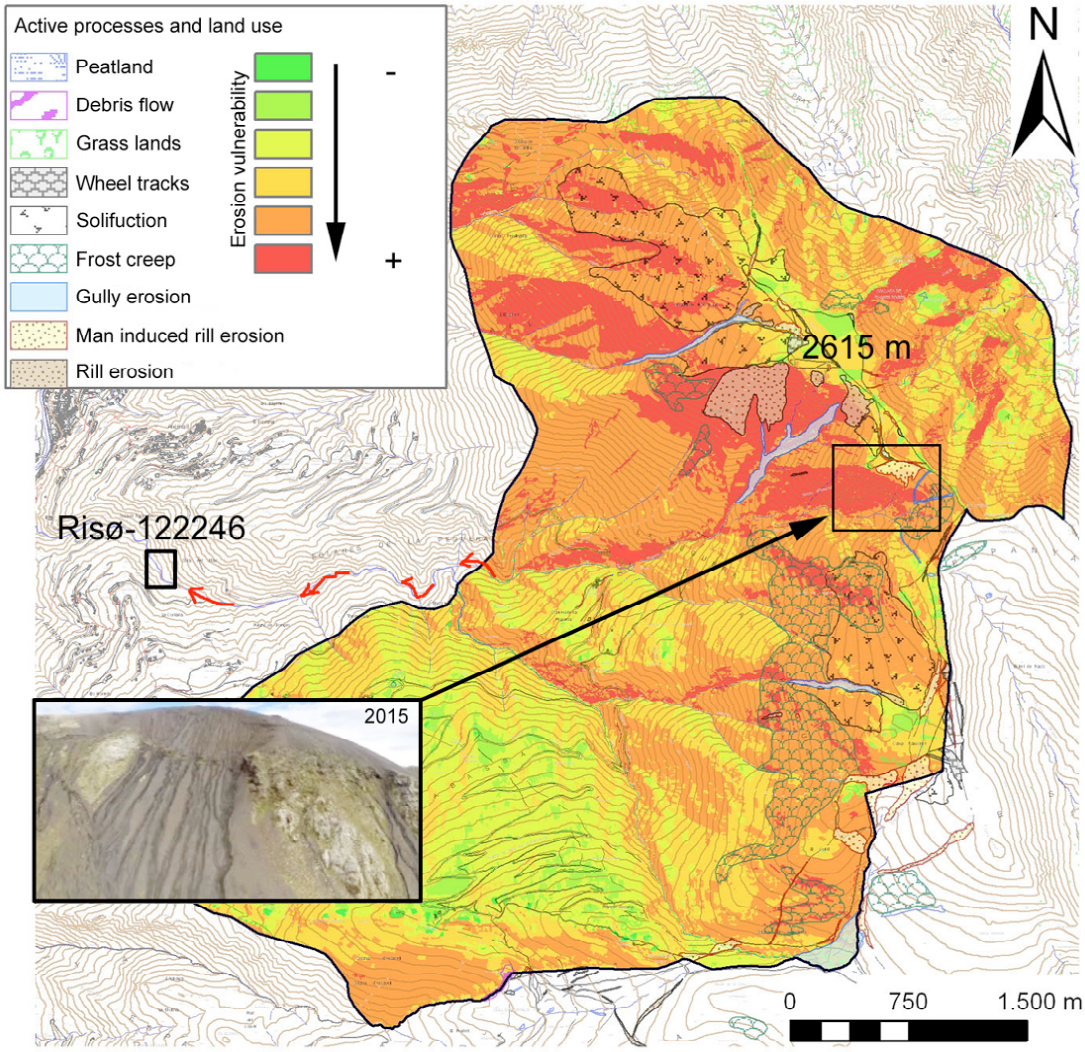

Fig. SM37 – Figure shows the upper basin vulnerability of the Auvinyà creek and the position of Faucelles site (sample 122246). A heavy thunderstorm (71 litres/hour) produced rill erosion on the 22nd of July 2015, affecting the upper basin and causing local flooding and bed-load sedimentation in the main village of Sant Julià de Lòria. (Andorra Igeotest Ltd. internal report num. D-010-ACSJ-036.11.08 held by the Marcel Chevalier Earth Science Foundation).

6.10 ADRALL AND SANT PERE CODINET

Sant Pere Codinet site is an abandoned open pit excavation of a quarry active between 1996 and 2006, a couple of kilometres southward from the Adrall village. A sample from the man-disturbed Segre riverbed, on the way to Sant-Pere Codinet, still has an Qtz offset of 0.19 ± 0.03 ka (**Table SM5**). The ADRALL-4 sample (179 ± 15 ka) is from an intermediate terrace close to the Segre-Valira confluence with a local stream (Castellbó river, 625 m a.s.l.). The bottom of the terrace is actually buried, but a large outcrop from the N-260 highway is still available (**Fig. SM38**). It shows three layers, eroding each one the upper part of its previous finning upward cycle. At the start of each cycle, clasts of granitic lithology dominate in point bars, coming from the Segre-Valira discharge. The upper part of the terrace was under the influence of the local river (Castellbó River) because it is mainly formed by local lithology (shists), The same sandy layer was previously dated using TL (ADRALL-3 or LUM-26, 120.0±5.5), but it should be a minimum age (TL signal in saturation). A correlative terrace exposed at the Cal Tolse quarry (at 865 m a.s.l. in the Valira valley; **Fig. SM38**) also provided a similar TL age (LUM-27, 125±14 ka; **Table SM6**); TL samples from higher fluvial terraces (ADRALL-1 and ADRALL-2; Turu and Peña-Monnñe, 2006) were found clearly in signal saturation (Turu and Peña-Monné, 2006).

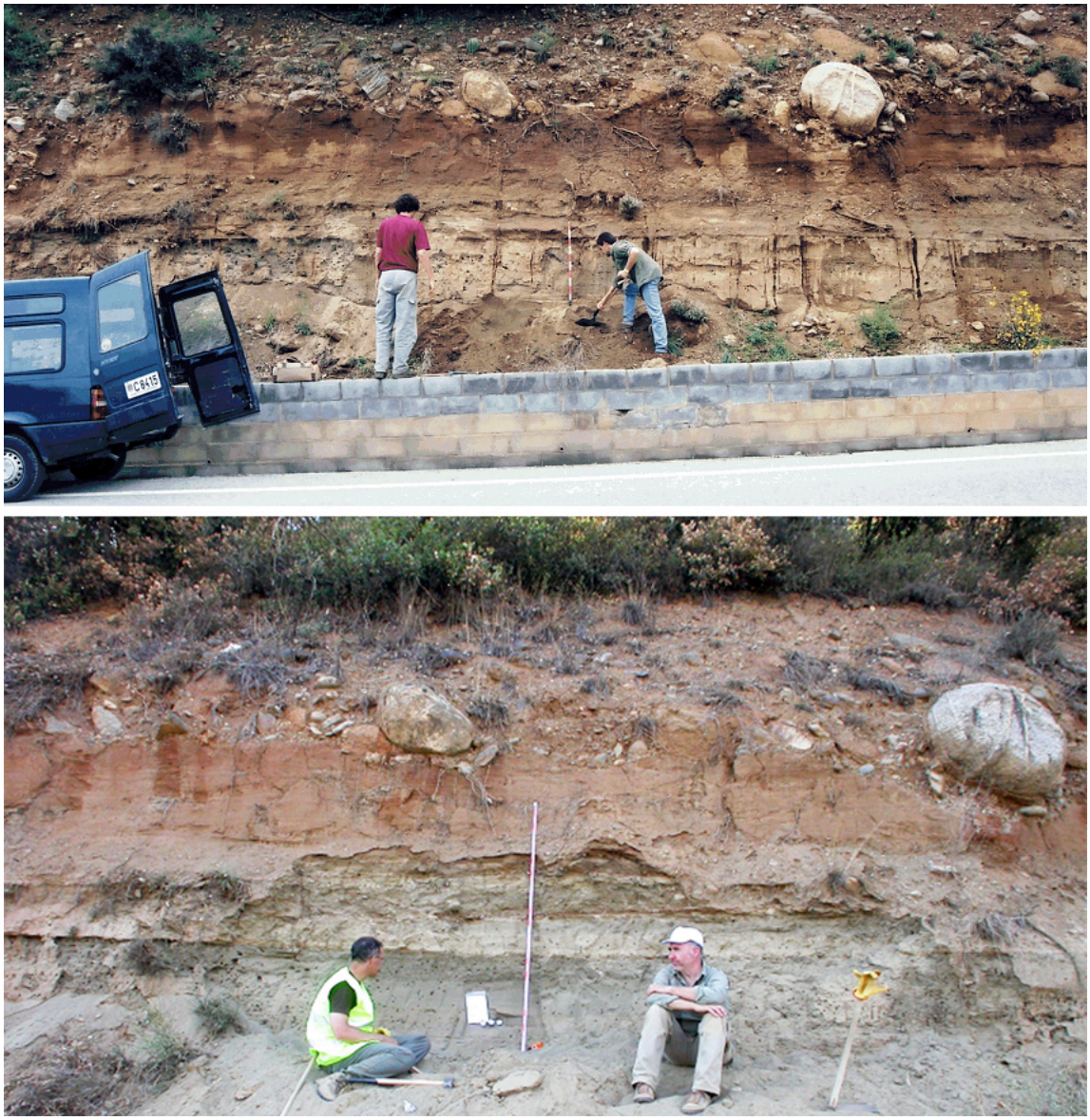

Fig. SM38 – Segre-Valira fluvial terrace sampling by May 2002 (upper picture), with Daniel Richter and Xavier Planas i Batlle, (LUM-27). Here, the exposure shows a lower bed of fine to coarse sands, and an upper bed comprises rounded boulders and imbricated cobbles and pebbles at Adrall. The picture from the bottom shows the same Segre-Valira fluvial terrace +35 m (a.r.b.). We were collecting the ADRALL-4 sample by the 9th September 2011. The exposure shows a lower bed of fine to coarse sands and an upper bed comprising rounded boulders and imbricated cobbles and pebbles.

6.11 GINEBROSA

As reported from the Turu and Bordonau (1997) inventory from http://llacglacial.ddns.net/), the La Cauba slope was dammed by the Arinsal glacier at its confluence with the Ordino glacier, and both with the Andorra glacier (Maximum Ice Extend episode, or MIE from Turu *et al*., 2017).

Outcrops (in Catalan, online in March 2022)

outcrop IV-2.3.1 - http://download1501.mediafire.com/0ohkevn94hrg/8yyapdt6r438822/Fitxa+IV-2.3.1.pdf

outcrop IV-2.3.2 - http://download1586.mediafire.com/7geg8877upjg/7sl4xea27etelac/Fitxa+IV-2.3.2.pdf

Three main depositional episodes are distinguished:

1) glacier advance and deposition of lodgement till.

2) glacier retreat and stabilisation, with deposition of rhythmites and predominance of fine grain sands.

3) glacier re-advance, producing the shearing and deformation of previous deposits and supraglacial till deposition.

Sandy layers from a kame terrace onlapped the overall deposits. Laminated sands are mixed with colluvium lenses (**Fig. SM39**). A layer of laminated sand was dated as 42 ± 8 ka (GINEBROSA-1; **Table SM5**). Over the bedrock (Unit 1), the sequence of the build-up of the Ginebrosa kame deposits and the evolution of the glacier is as follows:

Unit 2 – This unit consists of Imbricated gravels (Gt) and lenticular sand bodies (Shr) in a horizontal bedding pattern, although tilted around sloping bedrock margins (**Figure 7b** from the main text) and both covered by massive gravels (Gm). Deformation increases at the top of this unit, which is partially eroded (He) beneath a diamicton (Dmm) and supraglacial till (Dcs). An interpreted maximum regression surface (**Figure 7d, b**; MRS) is related to the retreat of the glacial ice that flooded Ginebrosa with the resulting meltwater.

Unit 3 - This unit overlaps the previous one. It comprises fine sediments deposited in the distal part of the kame (**Figure 7b**, Sh facies) during relative

glacier stabilisation when meltwater flooded the available space close to the glacier margin. Nevertheless, sands and silts grade to coarse gravels (Gp facies) deposited where meltwater streams fed the kame. Deposits consist mainly of clay silts, and sand lenses (Sh) interdigitated with colluvium. Coarse-grained sediment (offlap, **Figure 7b**) covers the fine-grain deposits, and its load promotes slumping of the clay–sandy sediments previously deposited. Near the former ice contact, these deformed beds include lenticular injections of cohesive clay caused by the pushing motion of the unstable Arinsal glacier. The age of interbedded laminated sand lenses is 42 ± 8 ka (GINEBROSA-1, **Table SM5**) and indicates ice damming during the second half of MIS 3 (**Figure 7a, b**).

Unit 4 - This unit only exists on the western side of Ginebrosa and is relatively thin (**Figure 7b**). Nevertheless, it represents the space-filling between the retreating glacier and the slope with imbricated gravels (Gt), overlapping the previous kame deposits in a downward trend, following a scour and fill process (**Figure 7b**). The boundary between units 4 and 3 is equivalent to a basal surface of forced (glacier) regression (BSFR surface) in sequence stratigraphy (Catuneanu, 2006).

Unit 5 - A Holocene post-glacial unit (**Figure 7b**) formed by fine-grained colluvium dates of 9.17 ± 0.15 ka cal BP using a ^{14}C AMS determination on bulk organic matter (GINEBROSA-2, **Table 3** from the main text).

Fig. SM39 – Sampling of the fine sand laminations intercalated with colluvium in the Ginebrosa site from La Cauba (La Massana, Andorra), the 11th September 2011.

7 THE NOGUERA RIBAGORÇANA AREA

Vilaplana (1983a, b), Vilaplana et al. (1983) and Montserrat-Marti (1985) reported a detailed description of the sedimentary deposits from lake Llauset (42º35'N-00º41'E, 2132 m a.s.l.).

7.1 THE LLAUSET PALAEOLAKE

In a relative small landslide scar, Vilaplana (1983a) described three main sedimentary units deposited above impure calcshists (Devonian age; Mey, 1965). The lowermost unit, light brown like (beige unit), shows laminated silts, interpreted by Vilaplana (1983a) as glacio-lacustrine rhythmites resulting from an oxygenated lake, quite some alkaline. The intermediate unit from Llauset is formed by intense yellow-like rhythmites, in which Vilaplana (1983a) reported submicroscopic goethite spherulites. Vilaplana (1983a) also observed gypsum phenoblasts up to 7 cm in this unit. Contact between these two units is transitional (Montserrat-Marti, 1985), and could be observed from a borehole core. The upper unit is black-coloured and is mainly formed by rhythmites. It follows paraconformably on top of the intermediate unit (Vilaplana et al., 1983; Montserrat-Marti, 1985), which might cause lateral thickness variability in the upper unit. Dropstones are common in all three units (Vilaplana, 1983a).

Vilaplana (1983a) reported two radiocarbon dates from the black-coloured unit (UZ-490, at 10.25 m depth, 20.930±0.310 ka BP, 24.467-25.886 ka b2k; and UZ-489, at 9.25 m depth, 12.620±0.160 ka BP, 14.235-15.484 ka b2k). Neighbouring samples are far distant in time. Vilaplana (1983a) remarked the low sedimentary rate (0.1 mm/a) between these two dated samples (^{4}C calibrated ages), while the post-glacial period is higher (0.62 mm/a). Similar values are reported from the Portalet peat bog (González-Samperiz et al., 2006) for full glacial conditions (0.08 mm/a) and the Holocene (0.64 mm/a). The radiocarbon ages reported by Montserrat-Marti (1985) from the upper unit range between 5975-6182 years b2k (β-4595; 5060±50 years BP; at 15 m depth), and 2170-1975 b2k (β-4594; 2050±80 years BP; at 2.5 m depth).

The sedimentary rate between these two dated samples for the Holocene is close to two times lesser (0.31 mm/a) than those reported by Vilaplana (1983a) and González-Samperiz et al. (2006). Sedimentary rates differences between sampled sites may refer to their relative position in the basin.

A detailed inspection of the available pictures present in Vilaplana (1983a) has been done for this work. Rx imaging from the core reveals truncation of the laminites at the bottom of the upper unit. Truncation may be related to a synsedimentary erosive surface (iceberg-drifts grooves, slump scars, ...); however, a general discontinuity may be discarded because it has not been seen in the field (Vilaplana pers. com.). Again detailed inspection of the upper unit from core Rx-imaging reveals that the density of dropstones (1 each 3 cm) is three times greater below the aforesaid truncation than above (1 dropstone each 7 cm). Vilaplana (1983a) invoke two origins for dropstones, an ice-rafted source or stones dropping from a frozen lake's melting surface. In that sense, dropstone-density differences may also refer to their ultimate origin.

7.1 LLESTUI AND ARTIGALLONGA-TINABRE

More precise datings come from the Llestui and Artigallonga lateral moraines complexes in the Noguera Ribagorçana glaciated valley. Vilaplana and collaborators (Vilaplana, 1983a, 1983b; Vilaplana et al., 1989; Vilaplana and Bordonau, 1989; Bordonau, 1992) reported a detailed description of the sedimentary facies from Llestui ice-dammed lake. Llestui is located further down, in the Llauset tributary valley at the upper Noguera Ribagorzana basin. The main valley is flanked by two morainic ridges represented by the Artigallonga (N-42º52'56'', E-0º45'31'', 1715 m a.s.l.) lateral moraine complex, located on the left side of the glaciated valley, and 600 m above the valley floor (Bordonau, 1992; Pallàs et al., 2006). The second morainic ridge is represented by the Llestui morainic complex, located on the right side of the valley (Vilaplana, 1983a; Bordonau, 1992; Pallàs et al., 2006), and about 70 below Artigallonga. Pallàs et al. (2016) performed several CRE (Terrestrial in-situ Cosmogenic Nuclides) on boulder populations from multiple moraines in the

Noguera Ribagorçana valley, and Bordonau et al. (1993) reported two dated samples from the glacio-lacustrine deposits of Llestui (Gif 8780, 18.240±0.600 ka BP, $^{13}\delta$ = -21.68, 20.612-23.497 ka b2k; Gif 8778, 21.650±0.900 ka BP, $^{13}\delta$ = -20.42, 23.993-27.671 ka b2k). The chronology spans GS-3 to GS-2c; however, the stratigraphic inversion in ^{14}C data makes its interpretation difficult. The early explanation from Bordonau *et al*. (1993) focused on the ^{14}C production of uncalibrated dates. However, Pallas et al. (2006) avoided calibrating samples Gif-8780 and Gif-8778 from Bordonau et al. (1993), providing an incomplete discussion. We recalculate the CRE new ages (**Table SM8**) following Nishiizumi et al. (2007). Correcting the exposure age of samples TIN01, ART02 and ART03, we obtained 26.9 +/- 6.2 ka (TIN01), 23.4 +/- 3.4 ka (ART02) and 20.8 +/- 5.1 ka (ART03) respectively. By the way, the calibrated ages from Llestui (Gif 8780 and Gif 8778) and the Tinabre-Artigallonga are quite the same, considering the error bars. Llestui and the Artigallonga's till were coevals when Llauset valley was free of ice (Vilaplana, 1983a; UZ-490, 24.467-25.886 ka b2k); thus, the main glacier should penetrate Llauset's valley and form the paleolake of Llestui.

Sample	Latitude N°	Longitude E°	Elevation (m) a.s.l.	Shielding	Exposure age (ka)	Uncertainty (ka)
TIN01	42,49	0,72	1301	0,968	**26,9**	**6,2**
ART02	42,55	0,76	1717	0,976	**23,4**	**3,4**
ART03	42,55	0,76	1717	0,976	**20,8**	**5,1**
IST01	42,61	0,77	1565	0,907	**18,0**	**2,3**
IST02	42,61	0,77	1565	0,919	**15,3**	**2,2**
IST03	42,61	0,77	1565	0,919	**20,2**	**3,9**
OBS01	42,60	0,79	1998	0,954	**20,5**	**3,3**
BES01	42,60	0,81	2137	0,926	**15,8**	**2,3**

Table SM8 – Samples from Pallàs et al. (2006) recalculated by using the online calculator formerly known as the CRONUS-EARTH project (http://cronus.cosmogenicnuclides.rocks/2.1/) for a supposed sample thickness of 2 cm, a density of 2.65 MN/m3 and an erosion rate of 1.5 mm/ka following Pallàs et al. (2006) descriptions. Samples TIN01, ART02, ART03 are plotted in Fig. 2 from the main text. Only the oldest date of IST01 to IST03 is in Fig. 2 represented (Santet moraine; Pallàs et al., 2006). Results from samples OBS01 and BES01 are also drawn in Fig. 2.

8 UNPUBLISHED FIELD DATA AND DATES

We insert keynotes from Jose Luís Peña-Monné from the Gavín lateral moraine complex in the Gállego valley and the Cinca valley (Cinca-Cinqueta glacier).

8.1 THE GAVÍN LATERAL MORAINE (GÁLLEGO RIVER)

Table SM7 report unpublished results from OSL datings performed on the external moraine ridge and in the internal ridge close to the Sia creek (following the Gavín Camping field).

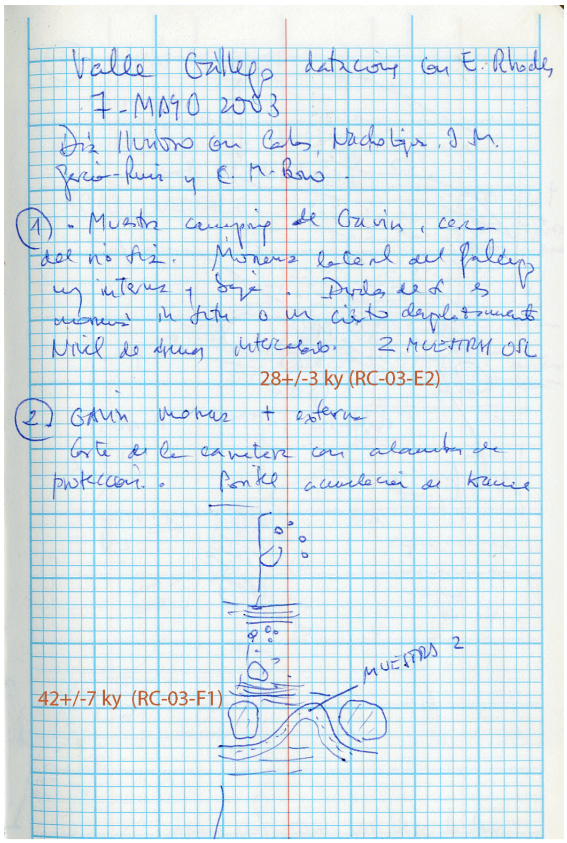

Jose Luis Pena-Monné (2021 com. pers.)

Figure SM40: – Sampling notes from the Gavín external moraine-kame complex. The coordinates are N42º37'15'' – W0º18'55.8'' — 1082 m a.s.l.

Literal traduction: Sampling in the Gállego valley with E. Rhodes. May 7th 2003. Rainy day with Carlos Sancho, Nacho López, J.M. García-Ruíz and Carlos Martí Bono.

1) Gavin camping sampling, near the river. Lateral moraine, the innermost and younger. Doubts about if it is an in-situ moraine or a slope slip. Sand level interspersed. Two samples were collected for OSL dating.

2) Road cut with protective wires at the external most Gavin lateral moraine allows kame deposit accumulation possible.

Field Ref.	Sample	Tubes	Dose (Gy)	Dr (GY)/ka	Lab. Code	Ages (yr)	Coments
RC-03-E2	X1595	3	62 ± 5	2.18 ± 0.11	OxL-1507	28,000 ± 3,000	GAVIN camping
RC-03-F1	X1596	5	72 ± 12	1.72 ± 0.08	OxL-1508	42,000 ± 7,000	GAVIN m. lat

Table SM7 – Results provided by the laboratory regarding Gavin. The dose rate (Dr) of "Gavin Camping" doubles the one from the lateral moraine (Oxf-1508) on the road N260. Coordinates are N42º37'02.2'' – W0º17'57.6'' — 920 m a.s.l.

8.2 THE SALINAS DE SIL (SOUTH-CENTRAL PYRENEES)

In this section, we insert a picture produced and commented on by Jose Luís Peña-Monné (**Fig. SM41**). Datings are from Lewis et al. (2009); however, it is interesting to note the deposit's internal deformation related to glaci-tectonics from a posterior Cinca-Cinqueta glacier advance.

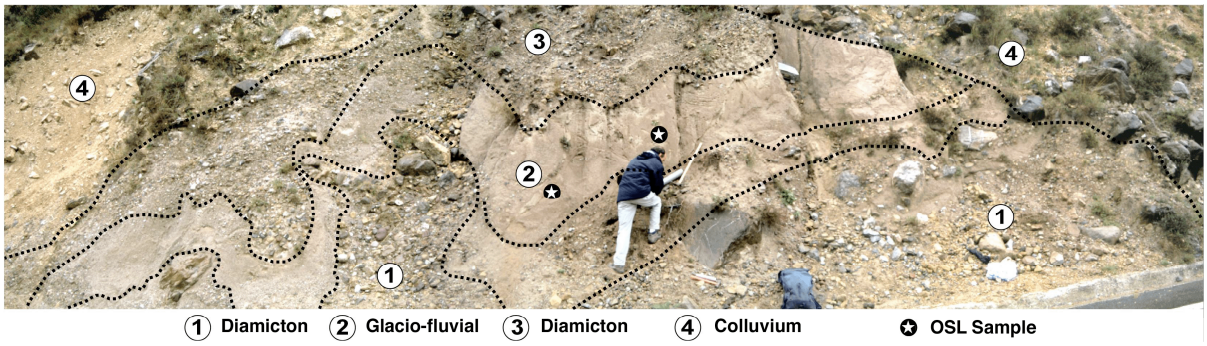

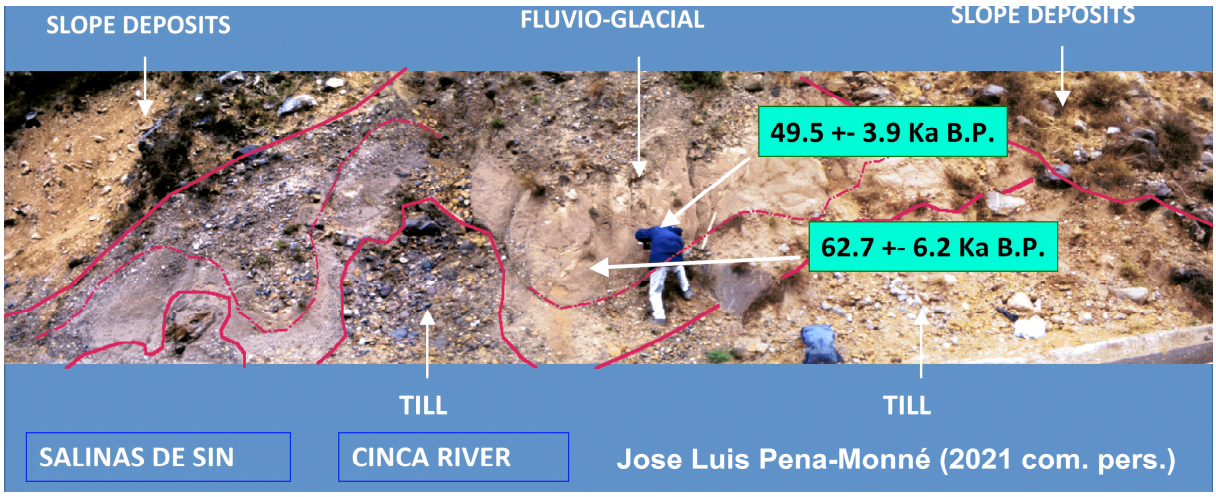

Figure SM41 – Salinas de Sin sketch picture shows two samples from the sandy layer were dated close to the highway A-138 (Km 73) trench. Coordinates are N42º35'5.1'' – E0º13'17.34'' – 825 m a.s.l.

9 REFERENCES

Bladé J.F., 1875. Études géographiques sur la vallée d'Andorre. Universelle. París (France), 97p

Bordonau J., Pous J., Queralt P., Vilaplana J.M., 1989. Geometría y depósitos de las cubetas lacustres del Pirineo. Estudios Geológicos 45 (1-2), 71-79.

Bordonau J., 1992. Els complexos glàcio-lacustres relacionats amb el darrer cicle glacial als Pirineus. Geoforma Ediciones, Logroño (Spain), 251 p.

Bordonau J., Vilaplana J.M., Fontugne M., 1993. The Glaciolacustrine complex of Llestui (Central Southern Pyrenees): A key-locality for the chronology of the last glacial cycle in the Pyrenees. Comptes-Rendus de l'Académie des Sciences, Paris, Série II 316, 807–813.

Blott S., and Pye K., 2001. Gradistat: a grain size distributions and statistics package for the analysis of unconsolidated sediments. Earth Surface Processes and Landforms: DOI: 10.1002/esp.261

Calvet M., 1996. Morphogénèse d'une montagne méditerranéenne, les Pyrénées Orientales; Thèse Doct. ètat lettres (1994) Univ. Paris I. Documents du BRGM, Orléans (France), 255, 1177 p.

Calvet M., 1998. Los complejos fluvioglaciares de Cerdanya-Capcir (Pirineos Orientales) y sus enseñanzas, in: Gómez-Ortíz, A., Pérez-Alberti, A. (Eds.), Las huellas glaciares de las montañas Españolas. UCS, Santiago de Compostela, pp. 263-291.

Calvet M., Delmàs, M., Gunnell, Y., Braucher, R., Bourlès, D., 2011. Le glaciaire du massif du Carlit et les systèmes morainiques terminaux de Cerdagne: Éléments de paléogeographie et de chronologie Quaternaire, In: Turu, V., Constante, A. (Eds.), El Cuaternario en España y áreas afines, avances en 2011, Andorra la Vella, pp. 21-25.

Catuneanu O., 2006. Principles of sequence strafigraphy. Elsevier Science, Amsterdam. 373 p.

Chevalier M. 1906. Sur les glaciers Pléisticènes dans les vallées d'Andorre. Comptes Rendues de l'Académie des Sciences, XLI, 662-663

Chevalier, M. 1907. Les glaciaires Pléistocènes dans les vallées d'Andorre. Revue Scientifique (revue rose-Sciences et Avenir), 23 (VII), 501-502

Farré D., 2000. Cartografía automática de mapas de riesgo de erosión utilizando sistemas de información geográfica. Master Thesis University of Lleida (Spain).

Fontboté J. M., Solé Sabaris L., Alimen H., 1957. Livret guide de l'excursion Nord Pyrenees. Fifth International INQUA Congress, 107, 45-167.

Gascón C., Turu V., 2011. Pont Trencat: la seqüència sísmica de 1427-1428 a la vall del Valira (Andorra-Alt Urgell, Pirineus Orientals), in: Turu, V., Constante, A. (Eds.), Cuaternario en España y áreas afines, avances en 2011, Andorra la Vella, pp. 127-131.

González-Sampériz P., Valero-Garcés B.L., Moreno A., Jalut G., García-Ruiz J.M., Martí-Bono C., Delgado-Huertas A., Navas A., Otto T., Dedoubat J.J., 2006. Climate variability in the Spanish Pyrenees during the last 30,000 yr revealed by the El Portalet sequence. Quaternary Research 66, 38–52. https://doi.org/10.1016/j.yqres.2006.02.004

Hartevelt J.J.A., 1970. Gology of the Upper Segre and Valira valleys, Central Pyrenees (Andorra/Spain). Leidse Geologische Mededelingen, 45, 167-236.

Jäger E., Zwart H.J., 1968. Rb-Sr age determinations of some gneiss and granites of the Aston-Hospitalet massif (Pyrenees); *Geol. en Mijnbow*, 47, 349-357

Jalut G., and Turu V., 2008. Le dernier cycle glaciaire-interglaciaire dans les Pyrénées: Englacement, Climat, Végétation. in: Canérot, J., Colin, J-P. Platel, J.P., Bilotte. M. (Eds.), Pyrénées d'hier et d'aujourd'hui, Biarritz, (France), pp. 145-161.

Johnson M.D., and Clayton L., 2005. Supraglacial landsystem in lowland terrain. In: Evams, D. (Ed.), Glacial Landsystems. Arnold, London (UK), 228-258

Krzyszkowski D., Zieliński T., 2002. The Pleistocene end moraine fans: controls on their sedimentation and location. Sedimentary Geology 149, 73-92. https://doi.org/10.1016/S0037-0738(01)00245-7

Llobet S., 1947. El medio y la vida en Andorra, estudio geográfico. Instituto Juan Sebastián Elcano-Estación de Estudios Pirenaicos, CSIC, Barcelona (Spain).

Mahaney W.C., Krinsley D.H., Razink J., Fischer R., Langworthy K., 2014. Clast rind analysis using multi-high resolution instrumentation. Scanning 38(3), 202-212.

Mey P.H.W., 1965. Geological Map of the Ribagorzana and Baliera Valleys, Central Pyrenees, Scale 1:25.000. Geological Institute, Leiden University.

Montserrat-Marti J., 1985. Estudi del Pleistocé superior i de l'Holocé en el rebliment sedimentari de l'Estany de Llauset (Pirineu Ribagorçà). MSC Thesis, Dep. Geomorfologia i Tectónica. Universitat de Barcelona (unpublished)

Nussbaum F., 1934. Die seen der Pyrenäen, Mitt. Nat. Ges., 184 p., Berna. (Translation Solé, L.: Els llacs dels Pirineus segons Nussbaum, Butlletí de la Institució Catalana d'Història Natural 36(2), 107-115, Barcelona 1936).

Nussbaum, F., 1956. Observations morphologiques dans la région de la Noguera Pallaresa, Pirineos 39-42, 57-97.

Nishiizumi, K., Imamura, M., Caffee, M.W., Southon, J.R., Finkel, R.C., Mcaninch, J., 2007. Absolute calibration of 10Be AMS standards. Nucl. Instrum. Methods Phys. Res. Sect. B Beam Interact. Mater. Atoms 258, 403-413.

Pallàs R., Rodés A., Braucher R., Carcaillet J., Ortuno M., Bordonau J., Bourlès D., Vilaplana J.M., Masana E., Santanach P., 2006. Quaternary Science Reviews 25, 2937–1963. https://doi.org/10.1130/G31164.1

Panzer W., 1926. Talentwicklung und eiszeitklima im nordostlichen Spanien, Abhandlungen der Senckenbergischen Naturforschenden Gesellschaft 39 (2) 141-182.

Penck A., 1884. Die Eiszeit iin den Pyrenäen [The ice age in the Pyrenees]: Mitteilungen des Vereins für Erdkunde zu Leipzig 23, 163-231.

Plata J.L., Rubio, F.M., 2007. Basic theory of the Magnetic Resonance Sounding Method. Boletín Geológico y Minero, 118 (3): 441-458 (http://www.igme.es/boletin/2007/118_3_2007/ART.%202.pdf)

Poblet J., 1990. Estructura herciniana i alpina del vessant sud de la zona axial del Pirineu central; Tesi doctoral, Facultat de Geologia de la Universitat de Barcelona (Spain), 604 p.

Poch R., 2022. Paleosols, una porta als paisatges del passat a través del microscopi. Institut d'Estudis Catalans, Secció de Ciències i Tecnologia, II, Barcelona (Spain), 31 p.

Prat M.C., 1980. Montagnes et vallées d'Andorre, étude géomorphologique. PhD thesis, Bordeaux III University, Bordeaux (France), 267 p.

Soler A., 1990. *Geologia i metalogènia del contacte sud del granit d'Andorra (Pirineu Central);* Tesi Doctoral de la Facultat de Geologia de la Universitat de Barcelona (Spain), 886 p.

Turu V., 1994. Datos para la determinación de la màxima extensión glaciar en los valles de Andorra (Pirineo Central), in: Arnáez-Vadillo, J., García-Ruiz, J.M., Gómez-Villar, A. (Eds.), Geomorfología en España, Logroño (Spain), I, pp. 256–273.

Turu V., Bordonau J., 1997. El glacialisme de les valls de la Valira del Nord (Principat d'Andorra): Síntesi d'Afloraments. Annals 1995 de l'IEA 41-104.

Turu V., Peña-Monné J.L., 2006. Ensayo de reconstrucción cuaternaria de los valles del Segre y Valira (Andorra - La Seu d'Urgell - Organyà, Pirineos Orientales): morrenas y terrazas fluviales, in: Pérez-Alberti, A., López-Bedoya, J. (Eds.), Geomorfología y Territorio: IX Reunió Nacional de Geomorfología USC, Santiago de Compostela, (España), pp. 129-148.

Turu V., 2011. Los complejos morrénicos terminales del Valira (Andorra-Alt Urgell), in: Turu, V., Constante, A. (Eds.), El Cuaternario en España y áreas afines, avances en 2011, Andorra la Vella, pp. 1-8.

Turu V., Ventura J., Ros X., Pèlachs A., Vizcaino A., Soriano J.M., 2011. Geomorfologia glacial del tram final de la Noguera Pallaresa i Riu Flamicell, in: Turu, V., Constante, A. (Eds.), El Cuaternario en España y áreas afines, avances en 2011, Andorra la Vella, 37-43.

Turu V., Calvet M., Bordonau J., Gunnell Y., Delmàs M., Vilaplana J.M., Jalut G., 2017. Did Pyrenean glaciers dance to the beat of global climatic events? Evidence from the Würmian sequence stratigraphy of an ice-dammed palaeolake depocentre in Andorra, in: Hughes, P.D., Woodward, J. C. (Eds.),

Quaternary Glaciation in the Mediterranean Mountains, Geological Society, London, Special Publications, 433(1), 111-136, https://doi.org/10.1144/SP433.6

Ventura J., Turu V., 2022. The Noguera Pallaresa glacier evolution (South–central Pyrenees), In: Oliva, M.; Palacios, D., Fernández-Fernández, J.M. (2021). Iberia, land of glaciers (4.2), Elsevier, pp. 87-121

Vilaplana J.M. 1983a. Estudi del glacialisme quaternari de les altes valls de la Ribagorça. PhD Thesis Universitat de Barcelona, 322 p.

Vilaplana J.M. 1983b. Quaternary Glacial Geology of Alta Ribagorça Basin (Central Southern Pyrenees), Acta Geològica Hispànica 18 (3-4), 217-233.

Vilaplana J.M., 1985. Les fases glacials del Quaternari superior en el sector nord-oest del Pirineu Andorrà, Revista d'Investigacions Geològiques 41, 67-82.

Vilaplana J., Montserrat-Martí J., Schüchter CH., 1989. Recent progress in Quaternary stratigraphy: The Lake Llauset sequence in the Spanish Pyrenees, in: Rose J., Schlüchter Ch. (Eds.), Quaternary Type Sections: Imagination or Reality?, A.A.Balkema, Rotterdam, pp. 113-124.

Vilaplana J.M., Bordonau J., 1989. Dynamique sédimentaire lacustre de marge glaciaire: Le paléolac de Llestui (Noguera Ribagorçana-Versant sud des Pyrénées). Bulletin de l'Association Française pour l'Étude du Quaternaire (AFEQ) 4, 219-224.

Walker M., 2005. Quaternary dating methods. John Wiley & sons, Ltd, West Sussex (England) 286 p.